Alma Mater Studiorum · Università di Bologna

Scuola di Scienze

Corso di Laurea Magistrale in Fisica del Sistema Terra

New Assessments of Global Sea Level Rise from Tide Gauges

Relatore:
Prof. Giorgio Spada

Presentata da:
Beniamino Rocchi

Sessione 3

Anno Accademico 2021/2022

Abstract

Estimates of global sea-level change rates based on observations from Tide Gauges (TGs) show a long-term global mean sea-level rise (GMSLR) of $1 \div 2\mathrm{mm\,yr^{-1}}$ for the 20^{th} century. The considerable scatter in these estimates is mainly attributable to the uneven distribution of the TG sites and to several physical phenomena that cause local sea level to deviate from the global mean, or to affect the TG record through land subsidence or uplift. The main cause of vertical ground motion on a regional space scale is the response of the Earth to past ice loads, called Glacial Isostatic Adjustment (GIA), which is often modelled and corrected for. In this work, a simple average approach was used to revisit two past estimates based on small sets of long, high-quality TG records in view of the longer record available, employing a newer GIA model (ICE-6G) from Peltier *et al.* [2015]. The value of GMSLR obtained from both sets is $(1.5 \pm 0.4)\,\mathrm{mm\,yr^{-1}}$. In addition, a much larger set of TGs was used to estimate the contemporary (post 1993) GMSLR using satellite estimates from Cazenave *et al.* [2018] as a benchmark, in an attempt to understand how a simple average approach could perform for larger sets. The resulting estimate of $(3.4 \div 3.5) \pm 0.2\ \mathrm{mm\,yr^{-1}}$ (depending on the GIA correction applied) is comparable to the satellite result of $(3.1 \pm 0.3)\,\mathrm{mm\,yr^{-1}}$.

Contents

List of Acronyms

GIA	Glacial Isostatic Adjustment
GMSL	Global Mean Sea Level
GMSLR	Global Mean Sea Level Rise
LGM	Last Glacial Maximum
MSL	Mean Sea Level
PSMSL	Permanent Service for Mean Sea Level
RLR	Revised Local Reference
rms	Root mean square
RSL	Relative Sea Level
sdom	Standard deviation of the mean
SLE	Sea Level Equation
TG	Tide Gauge
wrms	Weighted root mean square

List of Figures

List of Tables

Chapter 1

Introduction

The increasing concerns regarding climate change and global warming since the '70s made the issue of determining sea-level change rates a hot topic within the scientific community as well as for the broader public [Church *et al.*, 2001]. Sea-level rise, combined with extreme events (*e.g.*, droughts, floods, cyclones) is regarded as a major threat in highly populated and industrialized coastal regions of the world (see *e.g.*, Anthoff *et al.* [2010]). The driving cause of sea-level variations on a secular time scale is the variation of ocean water volume, mainly associated with two different climate-related processes. The first is land ice melting (glaciers, ice caps and ice sheets, see *e.g.*, Bamber *et al.* [2018]) and other land-water reservoir changes, resulting in a net mass variation, the second is a volume variation with constant mass (known as steric contribution) due to the variation of temperature and salinity of the water column, resulting essentially in the thermal expansion of the ocean water (see *e.g.*, Levitus *et al.* [2012]).

Changes in the mass, temperature and density distribution of the ocean water due to uneven heating and precipitations and the resulting ocean dynamic lead to a high variability of the local sea level, which according to Cazenave & Nerem [2004] can be up to ten times the global spatial average. Consequently, local sea-level estimates and predictions are of primary interest when assessing hazards on coastal communities. On the other hand, averaging over the entire ocean surface provides the variation of

Global Mean Sea Level (GMSL), which provides informations on different quantities, such as changes in ocean density or the net mass variations of continental ice masses, which are often poorly constrained due to the difficulties in assessing the volume of the ice sheets (see *e.g.*, Mitrovica *et al.* [2001]).

Reconstructions from proxy data by Lambeck *et al.* [2014] and Yokoyama *et al.* [2018] show that after reaching a minimum sea level of ~ -130m during the Last Glacial Maximum (LGM) around 21 kyr ago, the sea level increased at a fast pace ($\sim$12 mm yr^{-1} on average) slowing down to a negligible rate for the last two to three thousands years (see the IPCC Sixth Assessment Report, Gulev *et al.* [2021]). The actual rates in more recent times are still debated. For a fairly detailed discussion regarding the accuracy of estimates during the last 6 thousands years see *e.g.*, Gehrels [2010].

The basis for estimates of 20$^{\text{th}}$ century sea-level rise revolves around the careful interpretation of the records of Tide Gauges (TGs) placed by dock authorities around the world to monitor local sea level. These records in some cases reach as far back as the beginning of the 19$^{\text{th}}$ century, but were not originally intended for scientific purposes, and this may give rise to several problems. Therefore, an important step consists in obtaining a quality-uniform dataset to base the GMSLR estimates on.

Furthermore, local trends are affected by a variety of processes that cause them to deviate from the global mean. These effects include climate related changes in ocean dynamics, variations of the Earth's gravitational field and rotational state related to the mass shift caused by the contemporary melting of ice caps (ice melt fingerprints) as well as vertical movements of the solid Earth caused by the elastic response of the Earth to past ice melting (Glacial Isostatic Adjustment, GIA), co-seismic deformations, or anthropogenic causes (see Woodworth [2006]). Most of these processes can in a first approximation be dealt with by carefully choosing which records to consider, as discussed more in depth in Chapter 2. The major exception is GIA, as it produces vertical land movements comparable with the GMSLR over most of North America and Europe, where the majority of long, high-quality TGs are located. Past GMSLR estimates based on TG records are displayed in Table 1.1, along with the period considered and the methods used to correct for GIA, the Table is inspired to Table 1 of Spada & Galassi [2012] with the addition of recently published works. Following the notation that will be introduced in Chapter 3, the values of the estimate are indicated by μ.

Table 1.1: Previous GMSLR estimates based on the TG record. μ represents the computed value of the GMSLR estimate.

Author [year]	μ ($\mathrm{mm\,yr^{-1}}$)	Period[a]	GIA correction[b]
Gutenberg [1941]	1.1 ± 0.8	1807-1937	-
Polli [1952]	1.1	1871-1940	-
Cailleux [1952]	1.3	1885-1951	-
Valentin [1954]	1.1	1807-1947	-
Lisitzin [1958]	1.1	1807-1943	-
Fairbridge & Krebs Jr [1962]	1.2	1900-1950	-
Lisitzin [1974]	1.1 ± 0.4	1891-1943	-
Kalinin & Klige [1978]	1.5	1860-1960	-
Emery [1980]	3	1936-1975	-
Gornitz *et al.* [1982]	1.2	1880-1980	-
" "	1.0	1880-1980	Geological
Barnett [1983]	1.5 ± 0.2	1903-1969	-
Barnett [1984]	1.4 ± 0.1	1881-1980	-
" "	2.3 ± 0.2	1930-1980	-
Gornitz & Lebedeff [1987][c]	0.6 ± 0.4	1880-1982	Geological
" "	1.7 ± 0.3	1880-1982	Geological
" "	1.2 ± 0.3	1880-1982	Geological
" "	1.0 ± 0.1	1880-1982	Geological
Peltier & Tushingham [1989]	2.4 ± 0.9	1920-1970	ICE-3G
Pirazzoli [1986]	Indeterminable	1807-1984	-
Stewart [1989]	Indeterminable	1807-1984	-
Trupin & Wahr [1990]	1.75 ± 0.13	1900-1979	ICE-2
Nakiboglu & Lambeck [1991]	1.15 ± 0.38	1820-1990	ANU models
Douglas [1991]	1.8 ± 0.1	1880-1980	ICE-3G
Emery *et al.* [1991]	Indeterminable	1807-1986	-

Continued on next page...

Table 1.1 – continued from previous page.

Author [year]	μ (mm yr^{-1})	Period^a	GIA correction^b
Shennan & Woodworth [1992]	1.0 ± 0.15	1901-1988 EU	Geological
Gröger & Plag [1993]	1.8 ± 0.1	1880-1980	-
Mitrovica & Davis [1995]	$1.1 - 1.6$	1880-1990	ICE-3G
Unal & Ghil [1995]	1.6 ± 0.4	1807-1990	ICE-3G
Davis & Mitrovica [1996]	1.5 ± 0.3	1856-1995 USE	ICE-3G
Peltier [1996]	1.94 ± 0.56	1920-1970 USE	ICE-4G
Peltier & Jiang [1996]	1.8 ± 0.6	1856-1995 USE	ICE-4G
Douglas [1997]	1.8 ± 0.1	1880-1980	ICE-3G
Cabanes *et al.* [2001]	1.6 ± 0.15	1955-1996	-
Church *et al.* [2001]	$1.0 - 2.0$	1910-1990	-
Peltier [2001]	1.84 ± 0.35	1880-1980	ICE-4G
Mitrovica *et al.* [2001]	1.5 ± 0.1	1880-2000	-
" "	1.8 ± 0.1	1880-2000	ICE-3G
Church *et al.* [2004]	1.8 ± 0.3	1950-2000	ICE-4G, L, M
" "	1.75 ± 0.10	1950-2000	ICE-4G
" "	1.89 ± 0.10	1950-2000	L
" "	1.91 ± 0.10	1950-2000	M
Holgate & Woodworth [2004]	1.7 ± 0.2	1948-2002	ICE-4G
Nakada & Inoue [2005]	1.5 ± 0.2	1900-2000	-
Church & White [2006]	1.7 ± 0.3	1900-2000	ICE-4G, L, M
" "	0.71 ± 0.40	1870-1935	ICE-4G, L, M
" "	1.84 ± 0.19	1936-2001	ICE-4G, L, M
Hagedoorn *et al.* [2007]	1.46 ± 0.20	1900-2000	ICE-3G
Wenzel & Schröter [2010]	1.56 ± 0.25	1900-2006	ICE-5G
Church & White [2011]	1.7 ± 0.2	1900-2009	ICE-4G, L, M
" "	1.9 ± 0.4	1961-2009	ICE-4G, L, M
" "	2.8 ± 0.8	1993-2009	ICE-4G, L, M
Hamlington *et al.* [2011]	1.97	1950-2009	ICE-5G
Ray & Douglas [2011]	1.70 ± 0.26	1900-2007	ICE-4G, ICE-5G
Meyssignac *et al.* [2012]	1.8 ± 0.4	1950-2009	ICE-5G
Spada & Galassi [2012]	1.5 ± 0.1	1880-2010	ICE-3G, ICE-5G, L
Jevrejeva *et al.* [2014]	1.9 ± 0.3	1900-1999	ICE-4G, ICE-5G
Hay *et al.* [2015]	1.2 ± 0.2	1901-1990	Ensemble
Dangendorf *et al.* [2017]	1.1 ± 0.3	pre-1990	ICE-5G
Frederikse *et al.* [2018]	1.5 ± 0.2	1958-2014	ICE-6G

Continued on next page...

Table 1.1 – continued from previous page.

Author [year]	μ (mm yr^{-1})	Period[a]	GIA correction[b]
Dangendorf *et al.* [2019]	1.6 ± 0.4	1900-2015	Ensemble
Frederikse *et al.* [2020]	1.56 ± 0.33	1900-2018	Ensemble

[a] Global data are used, unless otherwise stated (EU, Europe, USE, United States East coast). Only the overall period considered is shown, individual record can span shorter periods.

[b] Geological corrections are based on Holocene RSL curves. ICE-2 denotes the model in Peltier [1986]. L and M denote models developed by K. Lambeck and J. X. Mitrovica (see Church *et al.* [2004]). Ensemble means a probabilistic approach was applied to several instances of the same or different models, with slightly different parameters.

[c] The three estimates are based on different selections of TGs.

Since the launch of the TOPEX/Poseidon altimetry satellite in 1992, sea-level variations are routinely measured by high-precision altimetry satellites. Unlike TGs, which are placed along shorelines often in densely populated and subsiding areas, sea-level observations by satellite radar altimetry allow a nearly complete sampling of the sea surface and are not directly affected by land motion. Although sea-level estimates from altimetry data still require to be corrected for GIA, they are not affected by the local vertical crustal movements that directly contaminate the TG observations. The near closure of the sea-level budget since the early 2000s (via GRACE space gravimetry and ARGO floats [Cazenave *et al.*, 2018]) also allows for corrections linked to the changes in the Earth rotational and gravitational fields despite the relative shortness of these records (both missions have been operational since the early 2000s).

The spatial distribution and lack of uniformity in length and quality of the TG records raise the question of which TGs are to be considered for GMSLR estimates. The simplest approach is to identify a small subset of long and high-quality TGs in order to smoothen the possible time fluctuations that affect the individual records at higher frequencies (*e.g.*, Douglas [1997], Holgate [2007], Spada & Galassi [2012]). Different selection criteria and corrections have been applied to the TG records, resulting in several (although often overlapping) sets, which reflect the length and quality of the record at the time, and the understanding of the processes affecting the individual sites.

In view of the longer record available, two examples of TG subsets (Douglas [1997] and Spada & Galassi [2012]) are discussed and revisited with a more recent GIA model (ICE-6G, Peltier *et al.* [2015]), essentially confirming the results of Spada & Galassi [2012] for the rate of GMSLR (1.5 ± 0.1 mm yr^{-1}). The entire TG record is subsequently used to provide separate estimates of secular and contemporary GMSLR. The latter is compared with the results from Cazenave *et al.* [2018] of $(3.1 \pm 0.3)\,\mathrm{mm\,yr}^{-1}$ in an attempt to asses the accuracy of estimates from the entire TG record and make a preliminary investigation on the use of the entire TG record for secular rate of change of the sea level.

Chapter 2 describes the TG record and the main problems that must be accounted for in the choice of a subset, as well as the criteria used in Douglas [1997] and Spada & Galassi [2012]. The methods used for the estimates and the corrections applied to the dataset are layed out in Chapter 3. In Chapter 4 updated estimates for GMSLR are presented, discussed and compared. The entire TG record is used to attempt to separate a "contemporary" GMSLR (1993 to present time) to be compared with the altimetry results given in Cazenave *et al.* [2018] over the same time span, from a "secular" GMSLR (1900-2000). Some remarks on the limitations of the methods used and possible improvements are discussed in Chapter 5.

Chapter 2

The Tide Gauge Record

The Permanent Service for Mean Sea Level (henceforth referred to as PSMSL) collects and provides TG sea level data from individual national authorities since 1933 (Holgate *et al.* [2013]; PSMSL [2021]), with some sites extending back to the 18$^{\text{th}}$ century. Monthly averages are released as the "metric" data set, now consisting of 2362 records as received by national authorities. TGs measure sea level relative to a crustal reference point, *i.e.*, where the instrument is physically located. This reference point may be subject to vertical movements at rates comparable to the expected sea-level signal, so this set of data is not to be used for GMSL assessment. Sites for which a complete geodetic history is available can be reduced to a common benchmark and are released by the PSMSL as the "RLR" (Revised Local Reference) data set, consisting of 1576 records (retrieved May 3 2021). The site distribution is showed in Figure 2.1. Annual values in the RLR data set are only computed if at least 11 months with less than 15 daily observations missing are present. Both the metric and RLR sets come with supporting information providing a complete description of the gauge selection process and relevant metadata for each record, *e.g.*, relevant informations about instruments, their placement and corrections applied to the record. As an example, monthly and annual records for one site (Bermuda) are given in Fig. 2.2.

In order to assess long term global mean sea-level variations, an appro-

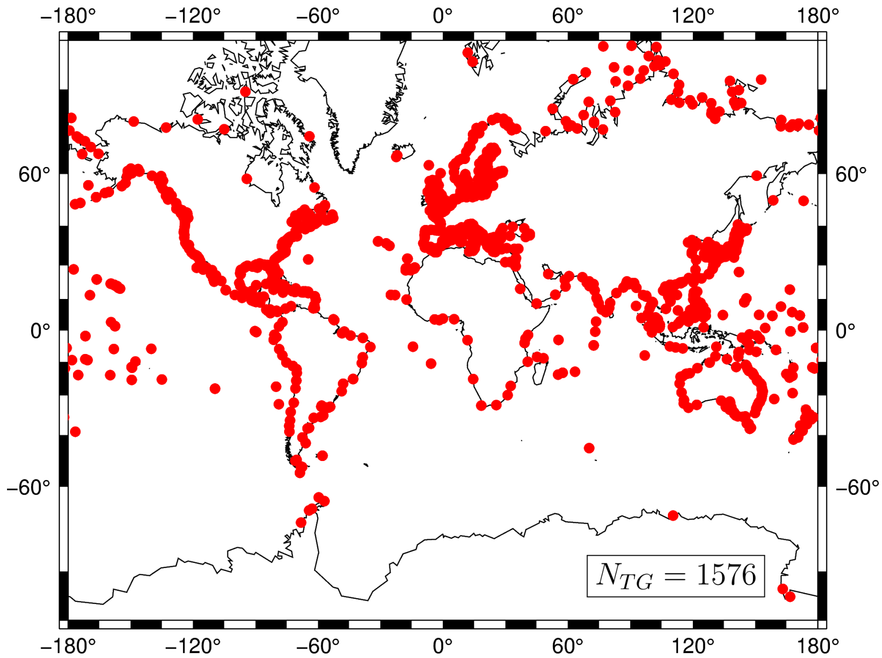

Figure 2.1: Distribution of the 1576 sites belonging to the RLR set of the PSMSL. N_{TG} is the number of TGs in the map.

priate subset of TGs must be defined. Up to now, the criteria applied to identify this subset have ultimately dealt with two underlying issues. The first, related to the instrumental nature of the TGs, is the need to properly deal with vertical land movements, involving a careful evaluation of the history of the TG sites, as well as a quality check of single records. The second, related to the sparse distribution of TGs and their different length and completeness, is the response of different TG ensembles to oscillations of the record in response to several known phenomena, such as atmospheric pressure or shifts in climate patterns.

Three main TG subsets are considered in this work: the first is the one used in Douglas [1997] (hereafter referred to as the D97 set). The second is a revised version proposed by Spada & Galassi [2012], based on the application of different GIA models to the D97 set. The third is the set considered in Spada & Galassi [2012] (hereafter referred to as the SG01 set). A summary of the criteria used in Douglas [1997] and in Spada & Galassi [2012] is presented in Table 2.1.

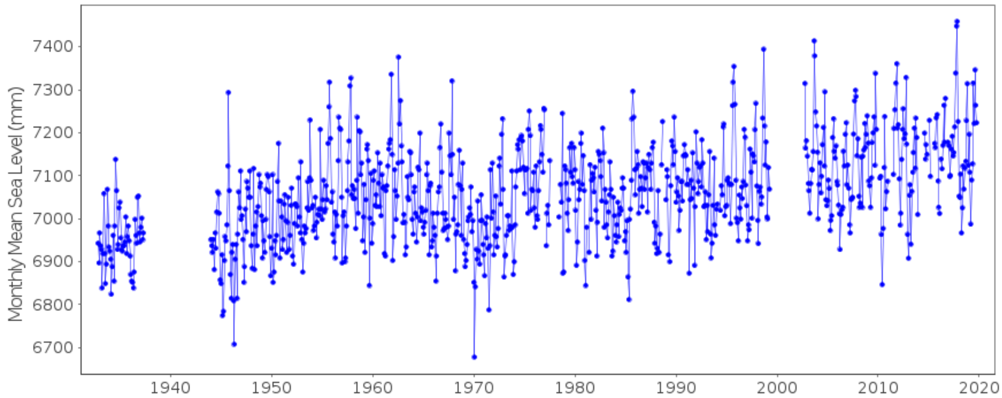

(a)

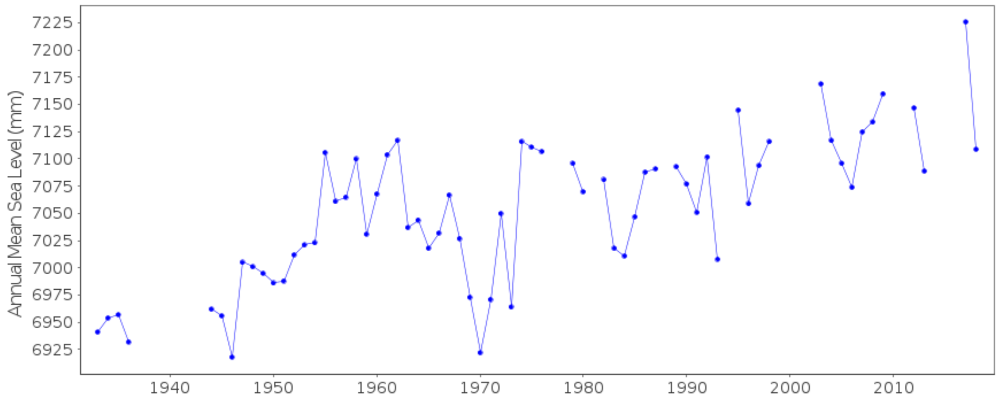

(b)

Figure 2.2: Monthly (a) and annual (b) records for the site of St Georges/Esso Pier (Bermuda) as provided by the PSMSL (adapted from `https://www.psmsl.org/data/obtaining/stations/368.php`

Finally, the whole RLR set of PSMSL is considered, in order to check how an unfiltered set performs, using these three datasets as a benchmark for the secular SLR, and estimates from satellite data for the contemporary SLR, *i.e.*, estimates for the 1993-2018 time period as given by Cazenave *et al.* [2018]. The statistical tools used for the estimates, as well as the corrections applied are discussed in Chapter 3.

2.1 Limitations of the TG record

2.1.1 Vertical land movements

TGs measure *relative* sea level, *i.e.*, the distance of the sea surface relative to a fixed point on the adjacent land. This means that any vertical movement of the solid Earth may affect the recorded sea level, resulting in a true signal which must be corrected or "decontaminated" to be useful for GMSL evaluation. Vertical movements due to local causes (*e.g.*, land sinking due to oil extraction, sediment compaction, urban development or other processes; co-seismic and post-seismic deformation; volcanic activity), are usually difficult to model. In theory, a careful choice of the TG site and an independent geodetic estimate of the land motion at the TG site could avoid most issues, however the use of TG series as scientific instruments is a relatively recent development. As a result, longer series often lack the quality control necessary to deal with these phenomena and a careful evaluation must be made for each site [Nerem & Mitchum, 2001]. Figure 2.4 shows some examples of time series with a few of the issues listed. These shall be considered in detail in Section 2.2.

Regional movements (in this context mainly GIA) can be modelled more successfully due to their greater spatial consistency. Before global GIA models were introduced by Peltier & Tushingham [1989], sea-level trends were often corrected by GIA trends extrapolated by geological sea-level records (*paleocoast lines*; *e.g.*, Gornitz *et al.* [1982]; Shennan & Woodworth [1992]) or not corrected at all. Starting from the 1990s GIA modelling has been routinely applied to most works, mainly based on the ICE-3G model of Tushingham & Peltier [1991] and subsequent versions.

Based on these premises, various authors identified different criteria resulting in several (although often overlapping) subsets of suitable TGs. It is worth noting that altimetry data are not directly affected by local vertical land motion as they measure *absolute* sea level relative to a reference frame with the origin coinciding with the Earth's centre of mass. However, they still need to be corrected for the global average GIA-component of the absolute sea level (see *e.g.*, Tamisiea [2011]). The physical meaning of the different GIA fingerprints is discussed in Section 3.2 more in detail.

2.1.2 Length, completeness and distribution of TGs

Local sea level recorded by single TGs is the superimposition of several signals characterized by different time scales, from semi-diurnal and diurnal tides to interannual and multidecadal oscillations related to long period tides, climate phenomena and mass movements in the Earth's mantle. There is no golden rule regarding the minimum length of a datum to be valid: in some fields, such as electrical engineering, the acquisition time is usually required to be at least ten times the oscillation, in order to avoid quantization errors. The lowest frequency oscillations are acknowledge to be longer than 20 years [Sturges & Hong, 2001], so this rule of thumb cannot be rigorously applied. As a matter of fact, starting from the work of Peltier & Tushingham [1989] it has been realised that a satisfactory trade-off can be reached accepting records longer than 50 years (70 years in Douglas [1991], 60 years in Douglas [1997] and Spada & Galassi [2012]). Poor sampling may be an issue also for records characterised by important gaps.

A partially related problem lies in the geographical distribution of TGs: oscillations over long distances end up having highs and lows in different times at different places, with a potential bias due to uneven sampling. The same problem arises when considering that GMSL changes happen at a very low frequency: suboptimal sampling could lead to confuse local sea-level changes due to long term variations in climate patterns or ocean dynamics with a GMSL change that is not actually real. Considering that the main drivers of GMSL (changes in salinity and heat content of ocean water and ice melting) exhibit a strong geographical variability, suboptimal sampling would introduce a potential bias. As discussed in Section 2.3 an additional problem arises considering that sea-level changes at the coasts do not necessarily reflect changes over the whole ocean, due both to local wind-driven coastal dynamics (on a time scale of months) and to the overall dynamics of the ocean basins (on a time scale of years to decades). Sturges & Douglas [2011] concluded that for the purpose of GMSLR only the longest records should be considered in order to minimize the impact of these oscillations.

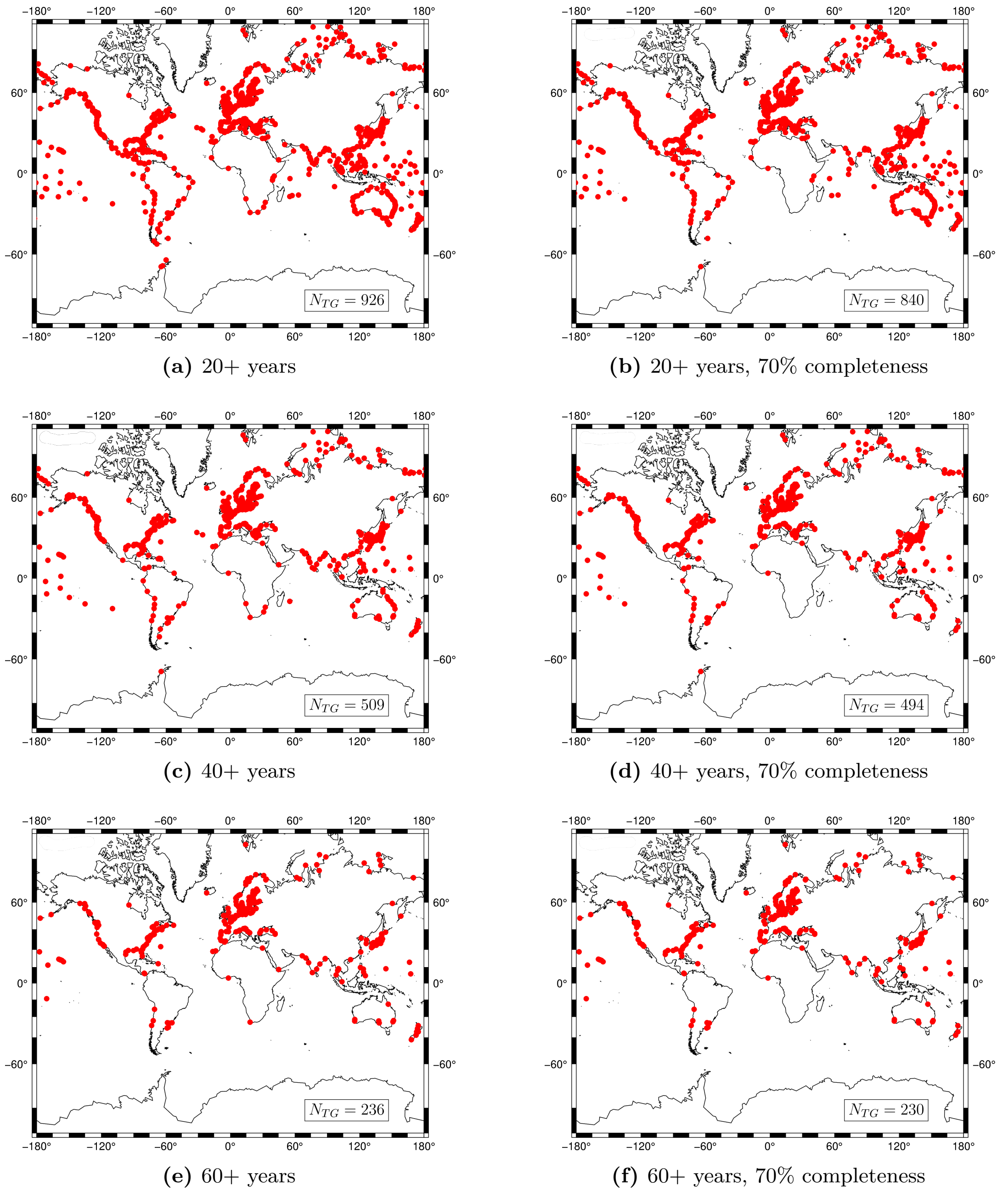

(a) 20+ years

(b) 20+ years, 70% completeness

(c) 40+ years

(d) 40+ years, 70% completeness

(e) 60+ years

(f) 60+ years, 70% completeness

Figure 2.3: Geographical distributions for TGs longer than 20, 40 and 60 years (a, c, e) and corresponding distributions for a completeness > 70% (b, d, f). The completeness is computed following Eq. (2.1).

Resulting distributions of RLR annual sites with records longer than 20, 40 and 60 years, as well as the corresponding distribution for sites with at least a 70% completeness are showed in Figure 2.3. Most sites end up being along the coasts of the Northern Emisphere, with some sites on islands in the open ocean, few of which are long enough to pass the 60 years threshold of Douglas [1997]. The Southern Emisphere and especially Africa are heavily under-sampled.This is a problem that must be acknowledged and will be discussed in Chapter 5.

2.2 Selection of a proper TG set

The three subsets herein considered essentially all derive from the criteria originally defined by Douglas [1991]:

(1) The TG series must be at least 60 years long,

(2) The TG must be at sites sufficiently distant from collisional tectonic boundaries,

(3) The series must have a sufficient completeness (80%),

(4) The series must be in reasonable agreement with nearby gauges at low frequencies, and

(5) The TG site must not belong to previously ice-covered area at the Last Glacial Maximum (LGM, ∼21,000ky years ago).

This set of criteria is an attempt to deal with the problems highlighted in the beginning of this chapter. Criteria (1) and (3) are the simple application of a quality check, discarding series with considerable gaps and ensuring a minimum length is met.

Criterion (2) is applied to remove sites potentially contaminated by seismic activity. An extreme example of the effect of seismic events is displayed in Figure 2.4d: the record shows a ∼18 cm jump (corresponding to a local ground subsidence) after the June 16, 1964 earthquake in Niigata

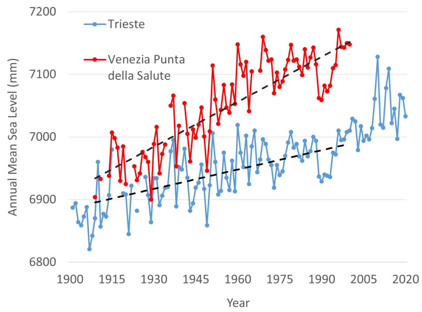

(a)

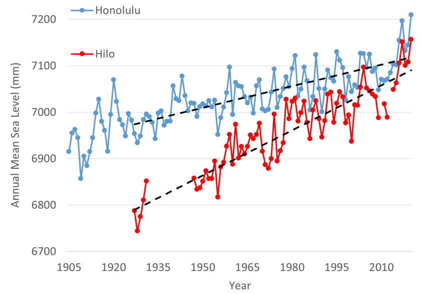

(b)

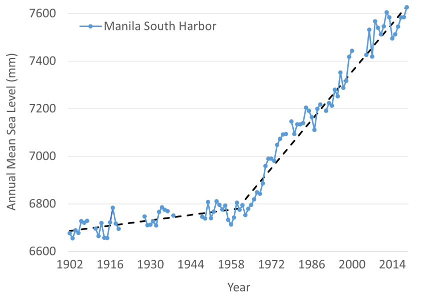

(c)

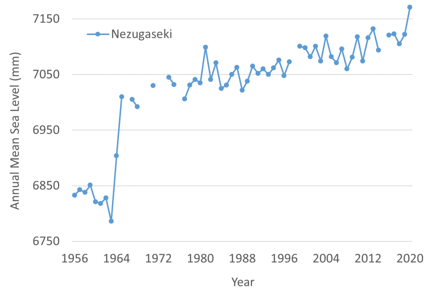

(d)

Figure 2.4: Examples of different physical phenomena that affect TG trends locally: (a) Records at Trieste and Venezia Punta della Salute in the northern Adriatic Sea. For the purpose of visualization, the Trieste record has been shifted down by 50 mm. The trends (computed for the same timespan) are of 1 mm yr^{-1} and 2.4 mm yr^{-1}, respectively. (b) Records at Honolulu and Hilo in Hawaii. The Hilo record has been shifted down by 100 mm. The trends are of 1.5 and 3.2 mm yr^{-1}, respectively. (c) Records at Manila South Harbor. Partial trends are 1.6 and 14.5 mm yr^{-1} before and after 1960. (d) Trend at Nezugaseki (Japan).

(Japan). Furthermore, a low frequency signal due to post-seismic relaxation may affect the whole record for an unknown amount, due to the high local uncertainty in post seismic modelling. The entire record must thus be rejected.

Criterion (4) above uses nearby TGs as a benchmark to check for local deviations of the MSL. The reasoning is that sites not far apart should be affected by the same dynamics on relatively long periods. As a consequence, the outliers should be investigated before being accepted or rejected. A couple of examples are discussed here. Figure 2.4a shows a comparison between the sites of Trieste (145 years, 85% completeness) and Venezia

Punta della Salute (91 years, 90% completeness). The two records show a clear agreement at higher frequencies, due to their proximity. However, when the mean trends are computed, Venezia shows a sea-level rise more that doubles that of Trieste ($2.4\,\mathrm{mm\,yr^{-1}}$ versus $1\,\mathrm{mm\,yr^{-1}}$, computed on the same timespan). This is due to a local subsidence most probably related to the pumping of freshwater for industrial use in the area near Venezia (Carbognin *et al.* [2004]). The site of Venezia must thus be discarded. Figure 2.4b compares the sites of Honolulu and Hilo, both located in the Hawaii. The same considerations made for Venezia apply, with the additional rate at Hilo caused by volcanic activity as the Big Island moves away from the Hawaii hotspot.

Criterion (5) above is placed in order to exclude sites that could be potentially too affected by GIA. This criterion proves to be the most critical of the set, as the exact pattern of uplift at the margin of the ice-covered area is extremely sensitive to changes in the ice melting history and lower mantle viscosity involved in the modelling [Lambeck *et al.*, 2014]. For this reason, Douglas [1997] cautiously extended the criterion to exclude sites adjacent to ice covered areas. However, this forces the exclusion of most high quality records in northern Europe and the East Coast of the USA, reducing dramatically the amount of usable records. Spada & Galassi [2012] exploited the wider choice of models available at their time to change the criterion to accept records with a GIA correction independent of the model used. Lastly, Spada & Galassi [2012] added a sixth criterion:

- TG series showing suspect accelerations and/or jumps, or affected by known human-driven effects must be discarded.

This was not formally expressed in Douglas [1997], but was still applied in Douglas [1991] for some sites, such as Manila (see Figure 2.4c), where the record shows an abrupt acceleration after ~ 1960. The almost tenfold post-1960 rate is attributable to land sinking following extensive harbour construction work as well as the increased deposition of river sediment (see `https://www.psmsl.org/data/obtaining/stations/145.php`). A summary of the criteria originally used for the D97 and SG01 sets is presented in Table 2.1.

Table 2.1: Selection criteria for the D97 and SG01 sets.

D97	SG01
(1) The TG series must be at least 60 years.	(I) It must contain at least 60 years of RLR annual records[a].
(2) The TG site must be sufficiently distant from collisional tectonic boundaries.	(II) See (2).
(3) The series must have a sufficient completeness (80%)[b].	(III) The series must have a sufficient completeness (70%)[b].
(4) The series must be in reasonable agreement with nearby gauges at low frequencies.	(IV) See (4).
(5) The TG site must not belong to previously ice-covered areas during the Last Glacial Maximum (LGM) $\sim$21 kyr ago or to the peripheral bulge adjacent to these areas	(V) The GIA correction should essentially be GIA-model independent[c]
(6) Not formally expressed in Douglas [1997]. See (VI).	(VI) TG series showing suspect accelerations and/or jumps, or affected by known human-driven effects should not be considered.

[a] For the details on what makes a valid annual RLR datum, see the introduction of this chapter.

[b] The definition of completeness in the two papers is formally different, as D97 uses monthly data whereas SG01 uses annual averages. The use of RLR data in the latter case makes this difference minimal. For the sake of consistency, where a measure of completeness is given, it is based on Eq. (2.1).

[c] Given two modelled GIA corrections, this is equivalent to imposing their difference to be lower than a threshold. In SG01 this threshold was set to $0.3\,\mathrm{mm\,yr^{-1}}$.

The subset found by Douglas [1997] consists of 24 TGs, one of which (Dunedin II in New Zealand) has not been considered here as it is not part of the RLR dataset and because its consistency and overall quality has been since re-evaluated by Hannah [2004]. In addition, another New Zealand site (Wellington II) has a considerably shorter RLR record than considered in Douglas [1997], starting in 1944 instead of 1901. This station was considered despite falling some year short of criterion (1) due to its considerably high completeness. Finally, following the example of Mitrovica *et al.* [2001] and Spada & Galassi [2012] the site of Lyttelton has not been considered because its rate is inconsistent with those at nearby sites. Figure 2.6a shows the distribution of the 22 remaining sites, with the annual records reported in Figure 2.5.

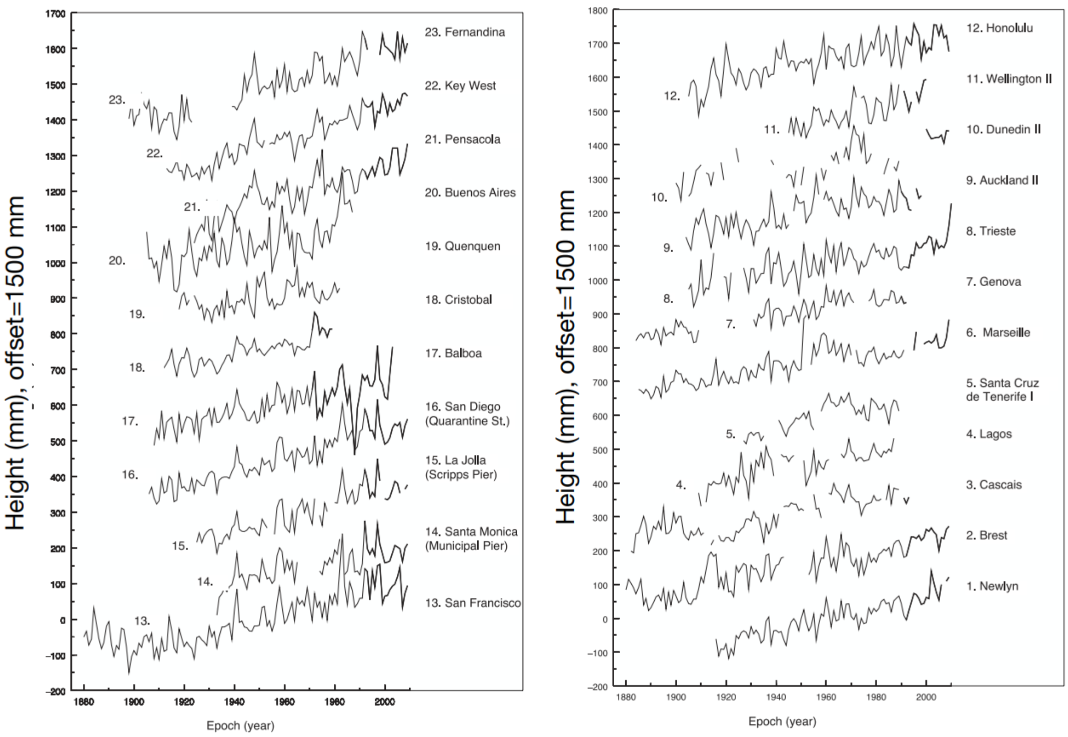

Figure 2.5: Annual records for the sites in D97 (from Spada & Galassi [2012]).

Spada & Galassi [2012] subsequently updated the estimate for the D97 set using the ICE-5G model Peltier [2004] and a model developed by Kurt Lambeck (see Lambeck *et al.* [1998] and subsequent improvements) together with the ICE-3G GIA model originally used in Douglas [1997]. Strict application of the original D97 criteria would justify the exclusion of seven sites (the four sites on the West coast and the three sites on the South-East coast of the US) due to the wider extension of the collapsing area under the new models used. This revised set (referred to as D97R hereinafter) consists of the remaining 17 sites (15 with the exclusion of Dunedin and Lyttelton) marked by a star in Table 2.2. Table 2.2 reports the current length and completeness of the sites in the D97 set, as well as the length considered in Douglas [1997]. The completeness of the k-th series is computed as the number of valid annual records N_k^V over the total length of the record span$_k$:

$$C_k = \frac{N_k^V}{\text{span}_k} \quad . \tag{2.1}$$

The average length of the records included in the D97 set increased from 83 years in Douglas [1997] to 106 years. Although the difference is roughly the same as the 25 years since Douglas [1997] was published, looking at the single records there is a considerable variability, with some TGs unchanged, some being much longer (up to over one century in the case of Brest) and in one case, even shorter (Wellington II).

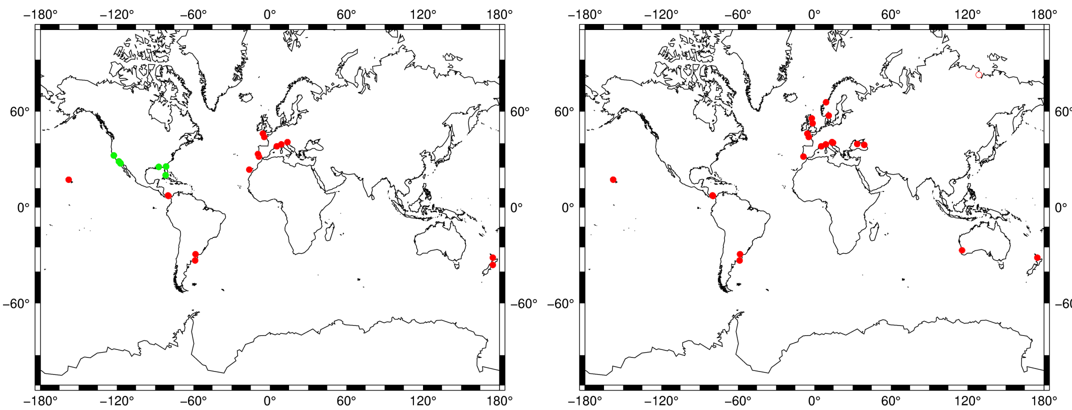

(a) D97 sites (b) SG01 sites

Figure 2.6: Geographical distributions of the sites in the D97 (a) and SG01 (b) sets. In (a) the sites in red identify the D97R set, with the 7 discarded sites displayed in green.

The SG01 set originally consisted of 22 sites, 13 of which are also part of D97. The site of Dunedin II has been excluded for the same reason stated before, bringing it down to 21 sites, 12 of which are included in D97 (see Table 2.3). The main differences with the D97 set are the inclusion of two sites in the Black Sea and one in Australia, the exclusion of the 7 sites already discussed in D97R, and the inclusion of 5 sites in Scotland, Northern Europe and Siberia based on criterion (V) (see Figure 2.6b). The average length of the sites considered is of 106 years, quite similar to that of D97.

Table 2.2: Sites in the D97 set.

Region	TG site	Period (yr-yr)	span_k(D97) (yr)	span_k (yr)	C_k
English Channel	Newlin	1916-2019	76	104	97%
	Brest	1807-2019	111	213	89%
Atlantic Ocean	Cascais	1882-1993	106	112	90%
	Lagos	1909-1987	81	79	87%
	Tenerife	1927-1989	64	63	89%
Mediterranean	Marseille	1885-2019	106	135	93%
Sea	Genova	1884-1996	105	113	75%
	Trieste	1875-2020	86	146	85%
New Zealand	Auckland II	1904-1998	85	95	97%
	Wellington II	1945-2000	87	56	95%
Pacific Ocean	Honolulu	1905-2020	86	116	100%
North America	San Francisco*	1855-2020	111	166	99%
West Coast	Santa Monica*	1933-2020	58	88	89%
	La Jolla*	1925-2020	66	96	95%
	San Diego*	1906-2020	85	115	97%
Central America	Balboa	1908-2018	62	111	99%
	Cristobal	1909-1979	61	71	100%
South America	Quequen	1918-1982	65	65	98%
	Buenos Aires	1905-1987	83	83	100%
South East	Pensacola*	1924-2020	68	97	96%
North America	Key West*	1913-2020	78	108	99%
	Fernandina*	1898-2020	94	123	83%

Sites belonging to the D97 set. span_k(D97) and span_k are respectively the total time span covered by the series in the original work and updated, C_k is the completeness of the series computed as of Eq. (2.1). The 7 sites denoted by a * are those ignored in D97R.

Table 2.3: Sites in SG01.

Region	TG site	Period (yr-yr)	span_k(SG01) (yr)	span_k (yr)	C_k
Siberia	Tiksi Bukhta	1949-2009	61	61	100%
Northern Europe	Heimsjo	1928-2020	82	93	88%
	Smogen	1911-2020	99	110	100%
Scotland	Aberdeen II	1862-1965	86	104	99%
	North Shield	1896-2017	114	122	90%
English Channel	Newlin*	1916-2019	94	104	97%
	Brest*	1807-2019	130	213	89%
Atlantic Ocean	Lagos*	1909-1987	79	79	87%
Mediterranean	Marseille*	1885-2019	125	135	93%
Sea	Genova*	1884-1996	113	113	75%
	Trieste*	1875-2020	106	146	85%
	Bakar	1930-2013	79	84	85%
Black Sea	Sevastopol	1910-1994	85	85	96%
	Tuapse	1917-2019	93	103	98%
Australia	Fremantle	1897-2020	113	124	90%
New Zealand	Auckland II*	1904-1998	95	95	97%
Central America	Balboa*	1908-2018	96	111	99%
	Cristobal*	1909-1979	71	71	100%
South America	Quequen*	1918-1982	65	65	98%
	Buenos Aires*	1905-1987	83	83	100%
Pacific Ocean	Honolulu*	1905-2020	105	116	100%

Sites belonging to the SG01 set. span_k(SG01) and span_k are respectively the total time span covered by the series in the original work and updated, C_k is the completeness of the series computed as of Eq. (2.1). The 12 sites denoted by a * are shared with the D97 set.

2.3 Effects of oscillations on local sea level

With regards to estimations of GMSLR, only long-term, global contribution to sea level are of interest. Even for sites unaffected by problems akin to those discussed in Section 2.2, several phenomena still affect the local records at different scales of time and space. The objective of this section is to discuss known phenomena that can cause the local sea level to deviate from the global average, and introduce possible solutions. As the exact determination of some of these phenomena, especially for the past, is difficult, many will be treated as noise, leading to the constrains in the length and distribution of records seen in the previous Section.

The first concern is over the instrumental measurements themselves. Wave motion at the coast can reach amplitudes of up to several centimetres depending on the local bathymetry and the wind forcing, raising the question of how to correctly measure the sea level. Earliest TGs were simple graduated sticks to be read at regular time intervals. Such readings are only accurate to a few centimetres, but can be used to successfully estimate daily tidal range and yearly sea level averages, if a sufficient number of daily measurements is available. Earliest examples of automated TGS employed a float connected by a wire to a recording device, floating in a *stilling well*, which acts as a mechanical low-pass filter eliminating higher frequency waves. Modern instrumentations usually measure the average of the sea level over a few minutes, either directly, with echo sounding, or indirectly, measuring the pressure of the water column over a point. Figure 2.7 gives a schematic description of a modern instrument.

Moreover, the sea level is in equilibrium with the weight of the column of air above, resulting in a sea surface depression in association with high pressure anomalies, and vice versa. According to Ponte [2006] this phenomenon (known as inverse barometer effect) can contribute to the sea-level change for values near $\pm 1\,\mathrm{mm\,yr^{-1}}$ in some sites, especially at higher latitudes. Corrections for the inverse barometer effect are commonly found to be effective at higher frequencies (periods shorter than a decade),

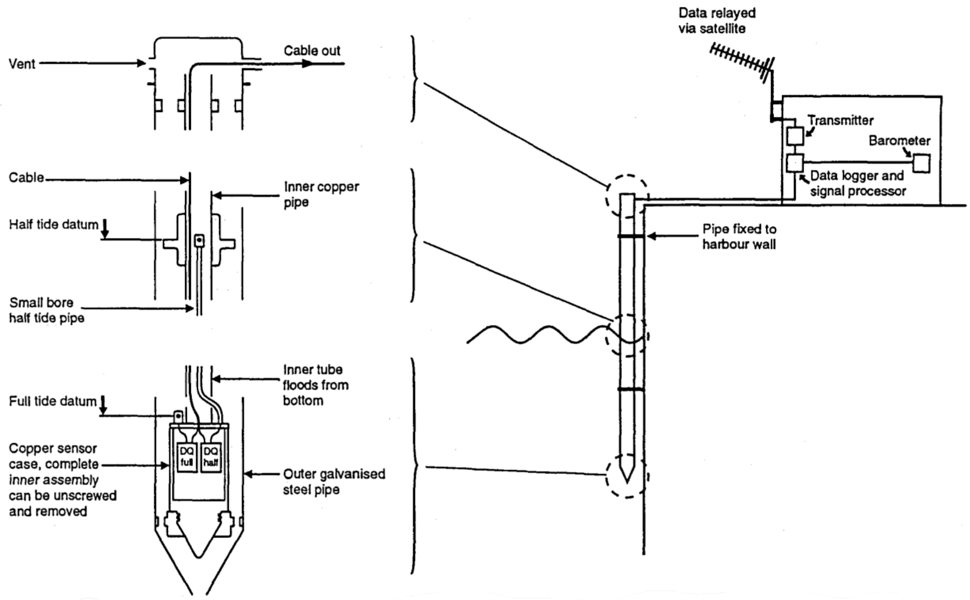

Figure 2.7: Schematic description of the ACCLAIM tide gauges employed at South Atlantic and Antarctic sites (1993) from Woodworth *et al.* [1996].

but as remarked by Sturges & Douglas [2011] their impact on GMSLR is negligible for the very long records considered in this work, if not for a possible improvement of its associated uncertainty.

Furthermore, a major problem in the use of TGs for GMSLR estimates is that TGs are, with very few exceptions, located on continental coasts. The implicit assumption that rates computed at the coast reflect the properties of the open ocean is not necessarily true. As a matter of fact, the Ekman transport due to longshore winds in the eastern side of ocean basins, especially on continental shelves, can be responsible for the piling of water nearshore or offshore, due essentially to the Coriolis force. This results in anomalies in the coastal sea level, which travel meridionally. These signals can travel westward in the form of long Rossby waves, taking years to cross the ocean basins. As an example, Sturges & Douglas [2011] found the considerable drop in the records of Western Europe between the end of the 1800s and the 1920s to be in agreement with longshore winds from the equator to higher latitudes. In the absence of precise models for these phenomena and other known climate systems that affect the sea level (such as El Niño Southern Oscillation) it is prudent to use only the longest records, in an attempt to dampen their effects.

The final major phenomenon affecting local sea level is the ongoing result of past ice melting, known as Glacial Isostatic Adjustment (GIA). The first, obvious consequence of ice melting on sea level is the resulting increment in the mass of the oceans. This increment, however, is not uniform over the globe, as the mass defect due to the melting affects the gravitational field of the Earth, so that the sea level rise is more pronounced far from the melted ice sheet. Lastly, the weight of the ice during the glacial period caused the areas covered by ice sheets to sink, and the adjacent areas to rise. With the ice load gone, the Earth gradually gets back to its original shape. Due to the high viscosity of the Earth's mantle, this process takes place over thousands of years, with a geometry and intensity dependent on the Earth's rheology and history of the ice load distribution. As reported

Figure 2.8: Measurement of a fossil tidal notch (Orosei Gulf, Sardinia, Italy) using a meter rod (from Benjamin *et al.* [2017]; photo: F. Antonioli). Tidal notches are an example of proxy used to build RSL curves. The height and the age of the notch are measured, providing the local relative sea level in the past. Similar procedures are used for other proxies.

in Table 1.1, the first attempts to correct for GIA relied on relative sea level (RSL) curves obtained by carbon dating of ancient shoreline features, such as ancient beach ridges or coral reef terraces (see Figure 2.8). GIA modelling relies on the solution of the Sea Level Equation (SLE) of Farrell & Clark [1976], a theory for the response of a visco-elastic, self-gravitating, non rotating spherical Earth to the melting of ice sheets. The models essentially implement different ice load histories and rheology of the Earth into the SLE in order to fit Holocene RSL curves. The reason why several models exist is that the SLE is an implicit equation, resulting in several sets of ice load histories and Earth parameters fitting the same curves.

Chapter 3

Methods

3.1 Sea-level trends

Due to the many sources of low-frequency oscillations presented in Section 2, it is appropriate to estimate the value of sea-level change at any given site through a simple linear regression (see *e.g.*, Taylor [1997]). Following Spada & Galassi [2012], the rate of sea-level change at the k-th TG is:

$$r_k = \frac{N_k^V \sum_j x_j y_j - \left(\sum_j x_j\right)\left(\sum_j y_j\right)}{N_k^V \sum_j x_j^2 - \left(\sum_j x_j\right)^2} \quad , \tag{3.1}$$

where the j index represents the year in a given record, so that $1 \leq j \leq N_k^V$ where N_k^V is the number of valid annual records, y_j is the average sea level at the corresponding year x_j, and the index k is associated to the TG ($1 \leq k \leq N_{TG}$, where N_{TG} is the number of TGs considered). The values of x_j and y_j are directly obtained from the annual RLR record provided by PSMSL. This is the appropriate stage to apply any correction, either to the yearly sea level y_j for correction with an interannual variability, or directly to the trends computed in Eq. (3.1) if the correction is considered constant in time. For the reasons displayed in Section 2.3, in this work only GIA corrections are applied, which are an example of the latter (see

Section 3.2).

Regardless of the correction, the formal uncertainty associated with the computed sea-level change is found by building a 95% confidence interval for r_k:

$$\sigma_k = \frac{SEE_k}{\sqrt{\sum_j (x_j - \bar{x})^2}}\, t_{0.975;\nu_k} \quad , \tag{3.2}$$

where

$$\bar{x} = \frac{\sum_j x_j}{N_k^V} \tag{3.3}$$

denotes the mean value of the x_j's and $t_{0.975;\nu_k}$ is the 0.975-th quantile of the Student's t-distribution with

$$\nu_k = N_k^V - 2 \tag{3.4}$$

degrees of freedom. The standard error of the estimate (SEE_k) in Eq. (3.2) is defined as the root mean square of the deviations:

$$SEE_k = \sqrt{\frac{\sum_j \left(y_j - y_j^{est}\right)^2}{\nu_k}} \quad . \tag{3.5}$$

The proper way to write the sea-level local rate of change at a given site is therefore:

$$\rho_k = r_k \pm \sigma_k \quad , \tag{3.6}$$

where r_k and σ_k are given by Eq. (3.1) and (3.2), respectively. The "best estimate" for GMSLR for a set consisting of a number N_{TG} of TGs can be computed as the arithmetic mean of the individual rates r_k, with:

$$g = \frac{1}{N_{TG}} \sum_k r_k \quad . \tag{3.7}$$

Douglas [1997] took the additional step of computing regional averages and averaging those again in order to minimize the possible error linked to the geographical distribution of the sites considered. Conversely, Spada

& Galassi [2012] did not consider them. The use of regional averages will be shortly discussed in Chapter 4, where it is shown that the difference amounts to a change in the second significant figure (one order of magnitude smaller than the error associated). Depending on the size and quality of the considered TG subset, alternative methods can be employed to estimate GMSLR. For instance, if the TGs are grouped geographically or just selected for their length, the GMSLR may be computed as the median instead of the mean, in order to minimize the influence of exceptionally large trends related to local processes (see *e.g.*, Emery [1980]; Gröger & Plag [1993]).

It is difficult to assign an uncertainty to the above estimates. The most appropriate choice for the small datasets used in this work would be the root mean square (rms):

$$\mathrm{rms} = \sqrt{\frac{\sum\limits_k (r_k - g)^2}{N_{TG} - 1}} \quad , \tag{3.8}$$

which characterizes the average uncertainty of the individual trends r_k. Since the individual uncertainties σ_k are not involved in this definition, it may be convenient to introduce them as weights in the rms to account for the large variability of the σ_k values. This is done by defining the weighted root mean square (wrms) as

$$\mathrm{wrms} = \sqrt{\frac{\sum\limits_k (r_k - g)^2 w_k}{\sum\limits_k w_k}} \qquad \text{with} \qquad w_k = \frac{1}{\sigma_k^2} \quad . \tag{3.9}$$

Another estimate of the error widely used in Earth Sciences is the standard deviation of the mean (sdom), which is the uncertainty of the mean and is defined as:

$$\mathrm{sdom} = \frac{\mathrm{rms}}{\sqrt{N_{TG}}} \quad . \tag{3.10}$$

The standard deviation represent the uncertainty of the best estimate g and is widely used for geophysical quantities (*e.g.*, sea surface temperature). However, it implies that data are uncorrelated, which is not strictly true in this case.

It is unclear how uncertainties are computed in Douglas [1997]. The author claims to have used the same statistical setup as Douglas [1991], where the rms was used. However, this is inconsistent with the given value of $(1.9 \pm 0.1)\,\mathrm{mm\,yr^{-1}}$. In fact, computing the rms of the regional average using the trends from table III of Douglas [1997] a value of $0.3\,\mathrm{mm\,yr^{-1}}$ is found.

In Spada & Galassi [2012] sdom was preferred, although rms and wrms were computed as well. In this work the rms will be used for the smaller datasets, with wrms and sdom given for the sake of completeness. When dealing with the entire RLR set, sdom will be preferred, as the ensemble better approximates a random distribution. The GMSL rate can thus be written as

$$\mu = g \pm \mathrm{rms} \tag{3.11}$$

or

$$\mu = g \pm \mathrm{sdom}\,. \tag{3.12}$$

The last two columns of Tables 3.1 and 3.2 compare the uncorrected rates provided in Douglas [1997] and Spada & Galassi [2012] to the respective updated values herein calculated. Differences of up to 0.4 mm arise, mostly due to the difference in the lengths considered. As an example, the site of Brest now reaches 73 years further back with a much flatter pace, resulting in a lower rate. Since in this work the rates are considered to be constant, the whole series has been considered (the issue of sea-level acceleration is briefly mentioned in Chapter 5). In a few cases (*e.g.*, Bakar) the time span considered is similar and the differences are attributable to the re-evaluation of single data or changes in the geodetic benchmark used by the PSMSL when building the RLR set.

Table 3.1: Local sea level rates for sites in D97.

Region	TG site	span_k(D97) (yr)	span_k (yr)	r_k(D97) ($\mathrm{mm\,yr^{-1}}$)	ρ_k ($\mathrm{mm\,yr^{-1}}$)
English Channel	Newlin	76	104	1.7	1.9 ± 0.1
	Brest	111	213	1.4	1.0 ± 0.1
Atlantic Ocean	Cascais	106	112	1.3	1.3 ± 0.1
	Lagos	81	79	1.5	1.6 ± 0.2
	Tenerife	64	63	1.5	1.6 ± 0.2
Mediterranean	Marseille	106	135	1.2	1.3 ± 0.1
Sea	Genova	105	113	1.2	1.2 ± 0.1
	Trieste	86	146	1.2	1.4 ± 0.1
New Zealand	Auckland II	85	95	1.3	1.3 ± 0.1
	Wellington II	87	56	1.7	2.0 ± 0.2
Pacific Ocean	Honolulu	86	116	1.5	1.5 ± 0.1
North America	San Francisco*	111	166	1.5	1.5 ± 0.1
West Coast	Santa Monica*	58	88	1.4	1.6 ± 0.1
	La Jolla*	66	96	2.1	2.0 ± 0.1
	San Diego*	85	115	2.1	2.2 ± 0.1
Central America	Balboa	62	111	1.6	1.4 ± 0.1
	Cristobal	61	71	1.0	1.4 ± 0.1
South America	Quequen	65	65	0.8	0.8 ± 0.2
	Buenos Aires	83	83	1.5	1.6 ± 0.2
South East	Pensacola*	68	97	2.2	2.6 ± 0.1
North America	Key West*	78	108	2.2	2.5 ± 0.1
	Fernandina*	94	123	1.8	2.2 ± 0.1

Sites belonging to the D97 set. span_k(D97) and span_k are respectively the total time span covered by the series in the original work and updated, r_k(D97) are the rates computed in the original work and ρ_k are the rates computed as of Eq. (3.6). No correction is applied to the rates at this stage. The 7 sites denoted by a * are those ignored in D97R.

Table 3.2: Local sea level rates for sites in SG01.

Region	TG site	span_k(SG01) (yr)	span_k (yr)	ρ_k(SG01) ($\mathrm{mm\,yr^{-1}}$)	ρ_k ($\mathrm{mm\,yr^{-1}}$)
Siberia	Tiksi Bukhta	61	61	1.6 ± 0.4	1.6 ± 0.2
Northern	Heimsjo	82	93	-1.5 ± 0.2	-1.2 ± 0.2
Europe	Smogen	99	110	-1.9 ± 0.2	-1.7 ± 0.1
Scotland	Aberdeen II	86	104	1.0 ± 0.1	0.6 ± 0.2
	North Shield	114	122	1.9 ± 0.1	1.9 ± 0.1
English	Newlin*	94	104	1.8 ± 0.1	1.9 ± 0.1
Channel	Brest*	130	213	1.4 ± 0.1	1.0 ± 0.1
Atlantic Ocean	Lagos*	79	79	1.4 ± 0.2	1.6 ± 0.2
Mediterranean	Marseille*	125	135	1.2 ± 0.1	1.3 ± 0.1
Sea	Genova*	113	113	1.2 ± 0.1	1.2 ± 0.1
	Trieste*	106	146	1.3 ± 0.2	1.4 ± 0.1
	Bakar	79	84	0.9 ± 0.2	1.1 ± 0.2
Black Sea	Sevastopol	85	85	1.3 ± 0.3	1.3 ± 0.2
	Tuapse	93	103	2.3 ± 0.2	2.4 ± 0.1
Australia	Fremantle	113	124	1.5 ± 0.2	1.7 ± 0.1
New Zealand	Auckland II*	95	95	1.3 ± 0.1	1.3 ± 0.1
Central	Balboa*	96	111	1.5 ± 0.1	1.4 ± 0.1
America	Cristobal*	71	71	1.4 ± 0.1	1.4 ± 0.1
South	Quequen*	65	65	0.9 ± 0.2	0.9 ± 0.2
America	Buenos Aires*	83	83	1.6 ± 0.2	1.6 ± 0.2
Pacific Ocean	Honolulu*	105	116	1.5 ± 0.1	1.5 ± 0.1

Sites belonging to the SG01 set. span_k(SG01) and span_k are respectively the total time span covered by the series in the original work and updated, ρ_k(SG01) are the rates computed in the original work and ρ_k are the rates computed as of Eq. (3.6). No correction is applied to the rates at this stage. The 12 sites denoted by a * are shared with the D97 set.

3.2 Sea level equation

The GIA "fingerprints" of sea-level change are evaluated solving the "Sea Level Equation" [Farrell & Clark, 1976] (SLE from here on). The SLE describes the response of a spherical, non rotational, visco-elastic Earth to variations of the ice loads. In its most basic form the SLE reads:

$$\dot{S} = \dot{N} - \dot{U} \quad , \tag{3.13}$$

where $\dot{S}$ is the relative sea level change, $\dot{N}$ is the absolute (geocentric) sea level change and $\dot{U}$ is the geocentric vertical displacement of the solid surface of the Earth. Figure 3.1 illustrates the quantities in play for TGs: as the instruments are affected by vertical movements of the ground with respect to the geoid, $\dot{S}$ is the appropriate GIA correction for TG estimates, whereas $\dot{N}$ is the GIA correction that must be applied to altimetry estimates (see *e.g.*, Tamisiea [2011]. The SLE for $\dot{S}$ can be expressed as:

$$S(\omega, t) = S^{gi}(\omega, t) + S^{e}(t) + S^{hi}(\omega, t) \quad , \tag{3.14}$$

where S is evaluated at a specific position $\omega = (\theta, \lambda)$, with θ the colatitude and λ the longitude, and time. The sea level is separated in a glacio-isostatic term $S^{gi}(\omega, t)$, an eustatic term $S^{e}(t)$ and a hydro-isostatic term $S^{hi}(\omega, t)$ (*e.g.*, Spada & Stocchi [2006]). The dependence of the two isostatic components on the position $\omega = (\theta, \lambda)$ denotes the fact that these two terms depend on the non-uniform Earth response to deformations. These are sensitive to the rheology considered for the interior of the Earth (as well as the ice load history), thus making the SLE an implicit equation. The eustatic term $S^{e}(t)$ on the other hand is the spatially uniform component that would be observed neglecting the rheology of the Earth as well as gravitational interactions between the ice sheets, the oceans and the solid Earth, and thus is a function of the ice volume variation only. The eustatic

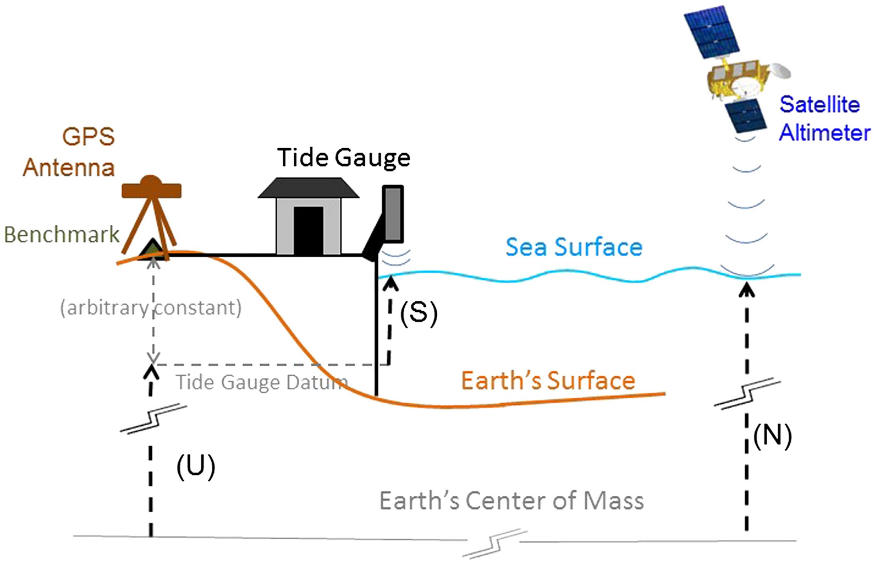

Figure 3.1: Sketch showing basic observational quantities and instruments related to sea-level investigations (from Wöppelmann & Marcos [2016]).

component can be written as:

$$S^e(t) = -\frac{m_i(t)}{\rho_w A_o} \quad , \tag{3.15}$$

where ρ_w is water density (assumed constant), A_o is the current area of the surface of the ocean and $m_i(t) = -m_o(t)$ is the ice mass variation which is equal to the opposite of the ocean mass variation. Regardless of any assumption about the Earth's rheological layering, an important property of the SLE is that its average over the ocean surface is equal to its eustatic component:

$$\overline{S(\omega, t)} = S^e(t) \quad , \tag{3.16}$$

where the overline indicates the spatial average (*e.g.*, Spada & Stocchi [2006]).

The GIA corrections are estimated implementing three previously published time histories of the late-Pleistocene ice sheets: ICE-3G(VM1) Tushingham & Peltier [1991], ICE-5G(VM2r) Peltier [2004], ICE-6G(VM5a) Peltier *et al.* [2015]. Each model consists of a spatio-temporal evolution of the ice thickness and a rheological model of the Earth's mantle, whose profiles and physical constrains are available in the respective original works. The models are implemented in the software SELEN version 4.0 Spada & Melini [2019] with a time discretization with steps of 1 kyr for ICE-3G and 500 yr for ICE-5G and ICE-6G. SELEN then uses the model to solve Eq. (3.14) numerically by a pseudo-spectral iterative approach. After testing the different parameters of the code an optimal trade-off between the time taken by the simulation and the precision achieved in the GMSL correction has been achieved setting a maximum harmonic degree $l_{max} = 128$ on a quasi-regular hicosahedral geodesic grid (Tegmark [1996]) with a spacing of ∼45 km and neglecting the sea-level variations associated to the rotational fluctuations of the Earth. Higher harmonic degrees, a denser grid and adding the effect of rotation have individually been applied and changed the GMSL estimate to less than 0.1 mm yr^{-1}, which is one order of magnitude lower than the uncertainty associated with the measure (regardless of which of the three possible estimate of the error is considered). The ICE-3G model employed a fixed shoreline (as for the original model) whereas for ICE-5G and ICE-6G the effect of the horizontal migration of shorelines is accounted for. Table 3.3 briefly summarizes the SELEN parameters for the models used in this work. The exact discretization of the ice history and the rheological models used is available in Spada & Melini [2019].

Table 3.3: SELEN configuration parameters for the three ice models used in this work.

Ice model	N	Δt	l_{max}	Moving shorelines
ICE-3G(VM1)	18	1.0 kyr	128	NO
ICE-5G(VM2r)	42	0.5 kyr	128	YES
ICE-6G(VM5a)	52	0.5 kyr	128	YES

Parameters N and Δt are the number of time steps and the time step length in the discretization of the ice height time history, respectively and l_{max} is the maximum harmonic degree of the integrand function.

For the combination of loads applied and viscosity profile considered in the models used, the Maxwell relaxation time of the mantle is of the order of a few thousand years (see *e.g.*, Schubert *et al.* [2001]). The rates of sea-level change can be then safely considered constant throughout the period of the instrumental sea-level record, at least until the role of transient rheological deformation will be fully determined. Thus, the local GIA component of the GMSL is simply the present day rate of sea-level change:

$$\dot{S} = \frac{dS}{dt}(\omega, t_p) \quad , \tag{3.17}$$

where S is the solution of Eq. (3.14) and $t = t_p$ the present time. Program SELEN computes the value of $\dot{S}$ for each cell in the grid.

Figure 3.2 shows maps of the present day value of $\dot{S}$ for the three realizations of the models considered. Noticeably, the peripheral forebulge for the ICE-3G model (shown in blue in Figure 3.2a) is localized in a small region inland, whereas its greater lateral extension in the other two models (Figures 3.2b and 3.2c) justify the rejection of sites along the West and East coast of the US in D97R. The GIA corrections for individual sites are obtained as the value of $\dot{S}$ in the grid cell they belong to. For the sake of completeness maps for the other GIA fingerprints computed are showed in Figures 3.3 (for the absolute sea-level change $\dot{N}$) and 3.4 (for the vertical displacement of the ground $\dot{U}$).

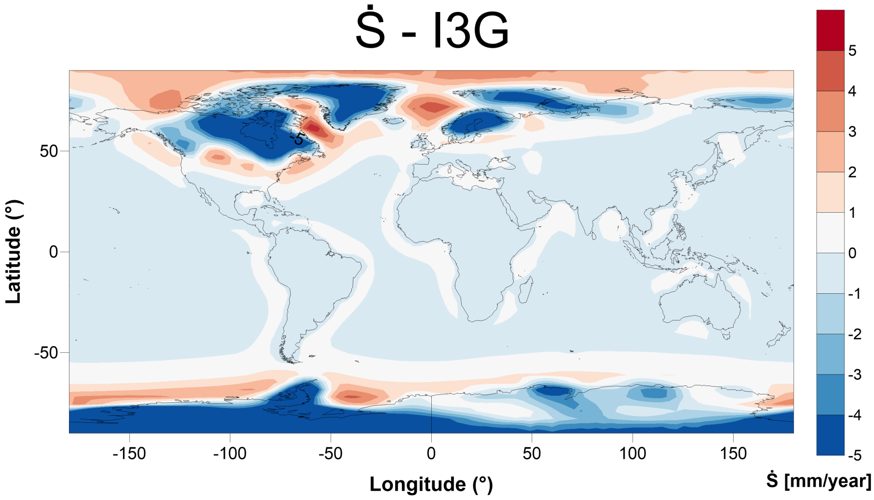

(a)

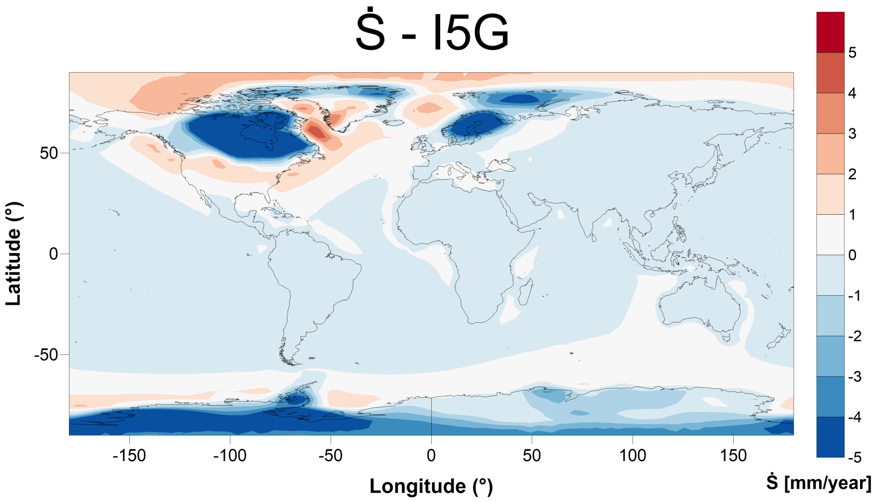

(b)

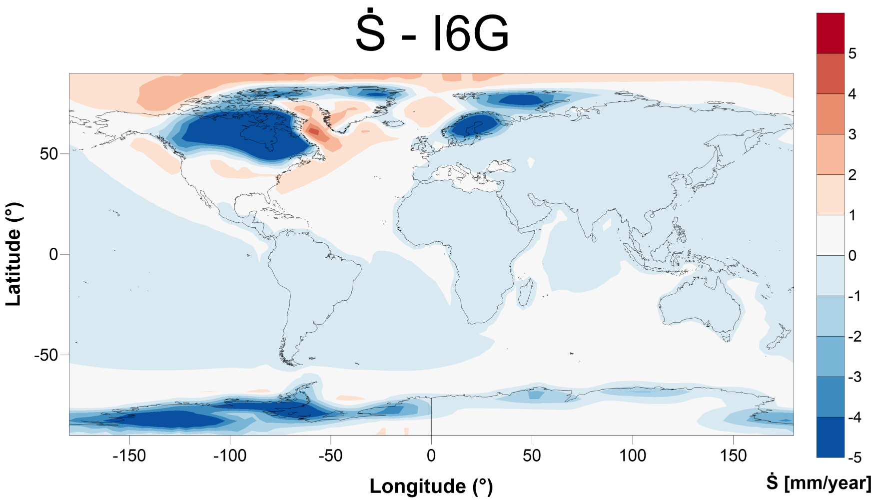

(c)

Figure 3.2: Rate of relative sea level change $\dot{S}$ for the ICE-3G (a), ICE-5G (b) and ICE-6G (c) models.

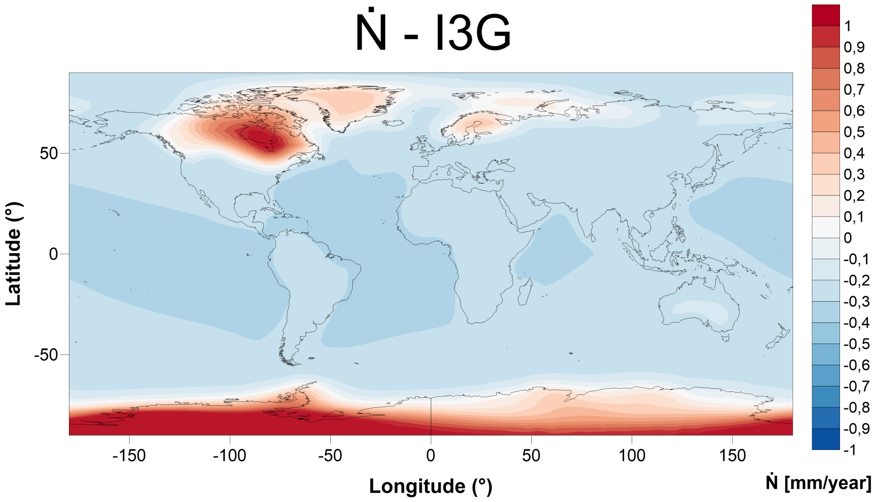

(a)

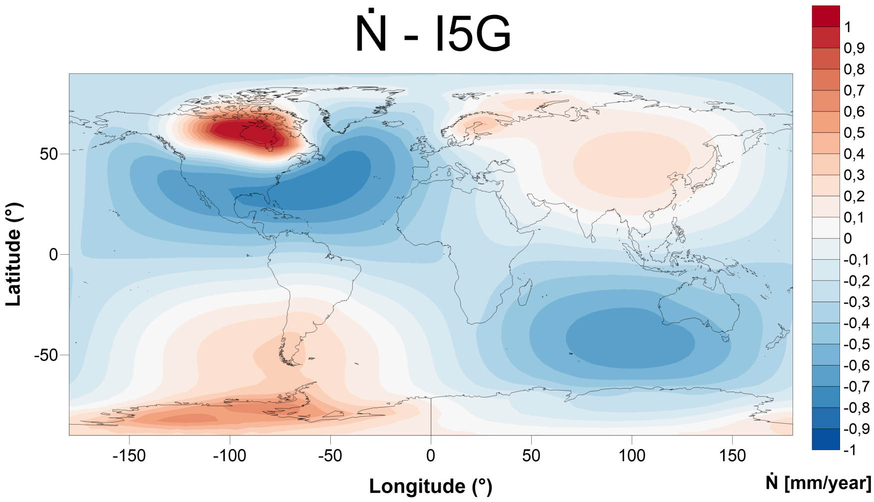

(b)

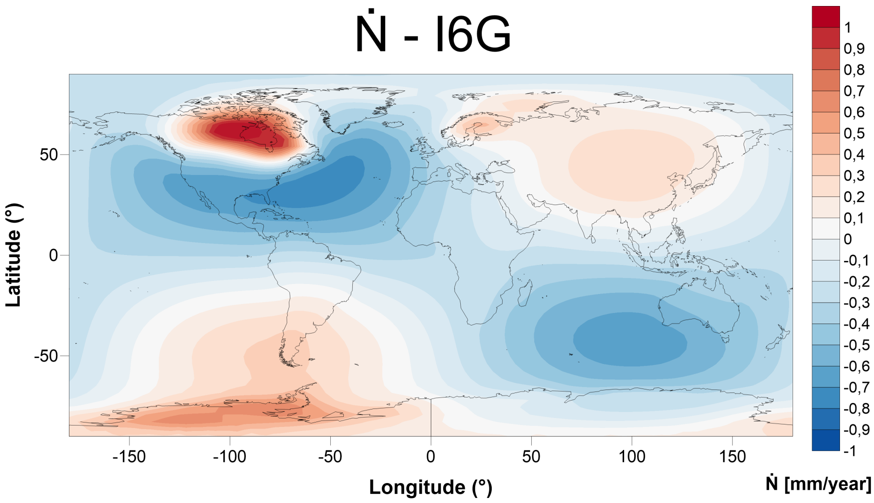

(c)

Figure 3.3: Rate of absolute sea level change $\dot{N}$ for the ICE-3G (a), ICE-5G (b) and ICE-6G (c) models.

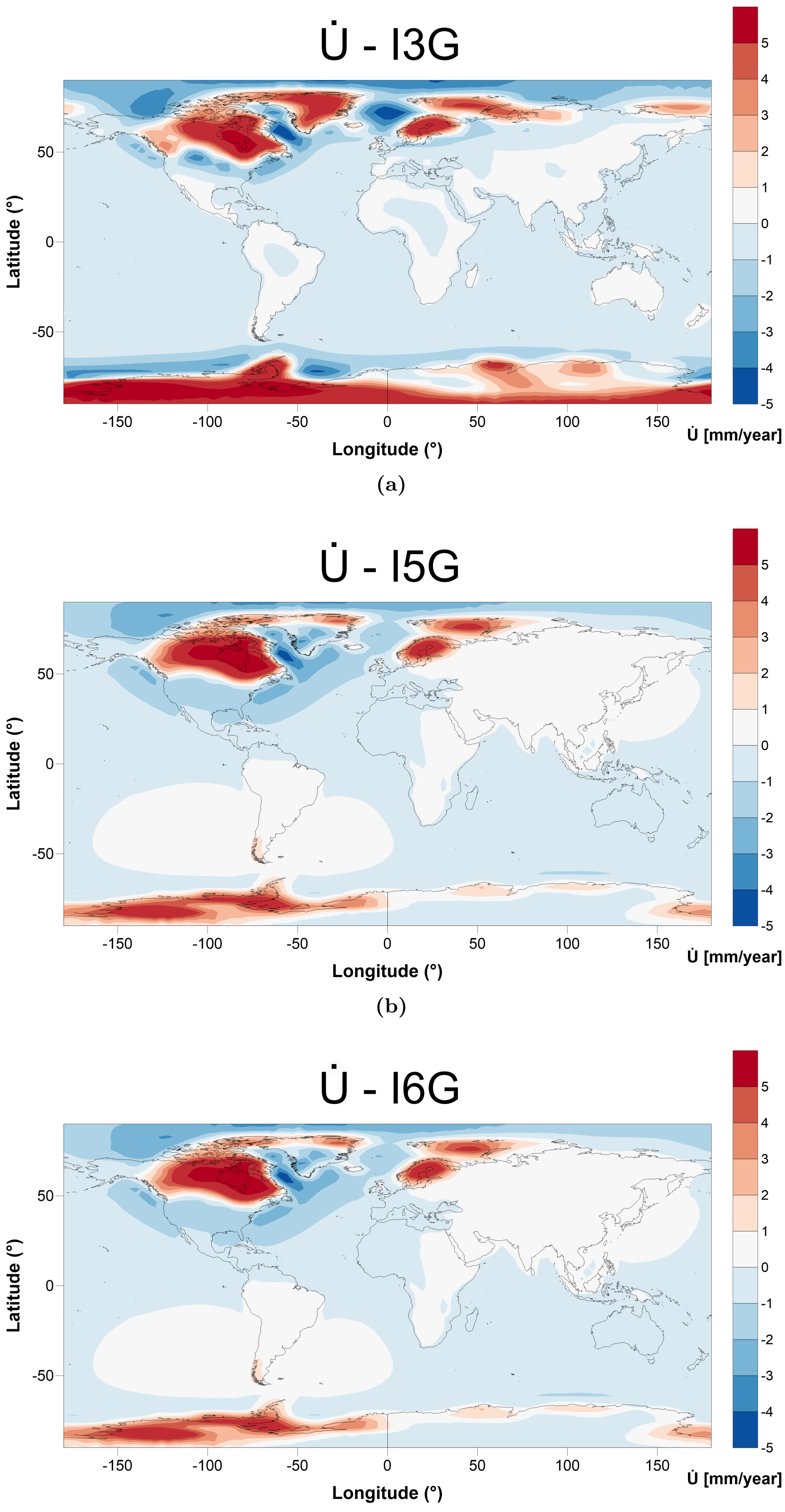

(c)

Figure 3.4: Rate of vertical displacement of the ground $\dot{U}$ for the ICE-3G (a), ICE-5G (b) and ICE-6G (c) models.

3.3 GIA corrections

GIA corrections are directly obtained from the outputs of SELEN as discussed in Section 3.2. Indicating the relative sea-level change $\dot{S}$ with r_k^{GIA}, Eq. (3.17) gives:

$$r_k^{GIA} = \dot{S} = \frac{dS}{dt}(\omega_k, t_p) \quad , \tag{3.18}$$

where $\omega_k = (\theta_k, \lambda_k)$ is the position (θ and λ are the colatitude and longitude, respectively) of the k-th TG and t_p is the present time. The computed GIA corrections for the individual sites are reported in Tables 3.4 (for the D97 and D97R sets) and 3.5 (for the SG01 set).

Denoting GIA-corrected quantities with a prime symbol, the corrected rates of sea-level change can finally be expressed as:

$$r'_k = r_k - r_k^{GIA} \quad , \tag{3.19}$$

where r_k and r_k^{GIA} are given by Eq. (3.1) and (3.18), respectively. Corrected rates will therefore be formally written as:

$$\rho'_k = r'_k \pm \sigma_k \quad , \tag{3.20}$$

where σ_k, given by Equation (3.2), is not primed because GIA-related uncertainties are not taken into account. The resulting corrected rates of local sea level ρ' for the D97 and SG01 sets are reported in Tables 3.6 and 3.7, respectively.

The equations for GMSLR and the different errors introduced are essentially unchanged, but for the substitution of r_k with r'_k. In particular:

$$g' = g - g^{GIA} \quad , \tag{3.21}$$

where

$$g^{GIA} = \frac{1}{N_{TG}} \sum_{k=1}^{N_{TG}} r_k^{GIA} \tag{3.22}$$

Table 3.4: Local uncorrected rates and GIA corrections for sites in the D97 set.

TG site	${\rho_k}^{(a)}$	$r_k^{GIA\,(b)}$		
		ICE-3G	ICE-5G	ICE-6G
	$(\mathrm{mm\,yr^{-1}})$	$(\mathrm{mm\,yr^{-1}})$	$(\mathrm{mm\,yr^{-1}})$	$(\mathrm{mm\,yr^{-1}})$
Newlin	1.9 ± 0.1	$+0.1$	$+0.2$	$+0.2$
Brest	1.0 ± 0.1	$+0.1$	$+0.2$	$+0.2$
Cascais	1.3 ± 0.1	-0.2	-0.1	-0.0
Lagos	1.6 ± 0.2	-0.2	-0.1	-0.0
Tenerife	1.6 ± 0.2	$+0.1$	$+0.0$	$+0.1$
Marseille	1.3 ± 0.1	-0.1	$+0.1$	$+0.0$
Genova	1.2 ± 0.1	-0.2	$+0.0$	-0.0
Trieste	1.4 ± 0.1	-0.2	-0.0	-0.1
Auckland II	1.3 ± 0.1	-0.4	-0.3	-0.2
Wellington II	2.0 ± 0.2	-0.5	-0.4	-0.3
Honolulu	1.5 ± 0.1	-0.2	-0.2	-0.1
San Francisco	1.5 ± 0.1	-0.1	$+0.6$	$+0.6$
Santa Monica	1.6 ± 0.1	-0.3	$+0.4$	$+0.5$
La Jolla	2.0 ± 0.1	-0.3	$+0.3$	$+0.5$
San Diego	2.2 ± 0.1	-0.3	$+0.3$	$+0.5$
Balboa	1.4 ± 0.1	-0.1	-0.2	-0.1
Cristobal	1.4 ± 0.1	-0.1	-0.2	-0.1
Quequen	0.8 ± 0.2	-0.2	-0.5	-0.4
Buenos Aires	1.6 ± 0.2	-0.5	-0.7	-0.5
Pensacola	2.6 ± 0.1	-0.0	$+0.6$	$+0.7$
Key West	2.5 ± 0.1	-0.1	$+0.1$	$+0.3$
Fernandina	2.2 ± 0.1	-0.0	$+0.5$	$+0.6$

[a] Rates of local sea level computed following to Eq. (3.6).
[b] Local GIA correction computed following Eq. (3.18).

is the simple average of the GIA corrections at TGs. The assumption in the GIA models that no recent ice melting happened implies this quantity to vanish. This is because in the SLE only the eustatic component of S is left on the global average (see Equation 3.16). Setting a constant melting contribution in Equation (3.15) implies $\dot{S}^e = \overline{\dot{S}} = 0$. However, this would only be observed in the presence of a regularly spaced and dense network of

Table 3.5: Local uncorrected rates and GIA corrections for sites in the SG01 set.

TG site	${\rho_k}^{(a)}$	$r_k^{GIA\,(b)}$		
		ICE-3G	ICE-5G	ICE-6G
	$(\mathrm{mm\,yr^{-1}})$	$(\mathrm{mm\,yr^{-1}})$	$(\mathrm{mm\,yr^{-1}})$	$(\mathrm{mm\,yr^{-1}})$
Tiksi Bukhta	1.6 ± 0.2	$+0.1$	-0.4	-0.3
Heimsjo	-1.2 ± 0.2	-3.4	-3.1	-2.9
Smogen	-1.7 ± 0.1	-2.6	-3.3	-3.0
Aberdeen II	0.6 ± 0.2	$+0.1$	-0.4	-0.3
North Shield	1.9 ± 0.1	-0.1	-0.3	-0.3
Newlin	1.9 ± 0.1	$+0.1$	$+0.2$	$+0.2$
Brest	1.0 ± 0.1	$+0.1$	$+0.2$	$+0.2$
Lagos	1.6 ± 0.2	-0.2	-0.1	-0.0
Marseille	1.3 ± 0.1	-0.1	$+0.1$	$+0.0$
Genova	1.2 ± 0.1	-0.2	$+0.0$	-0.0
Trieste	1.4 ± 0.1	-0.2	-0.0	-0.1
Bakar	1.1 ± 0.2	-0.2	-0.0	-0.1
Sevastopol	1.3 ± 0.2	$+0.3$	$+0.3$	$+0.2$
Tuapse	2.4 ± 0.1	$+0.0$	$+0.1$	$+0.1$
Fremantle	1.7 ± 0.1	-0.4	-0.3	-0.2
Auckland II	1.3 ± 0.1	-0.4	-0.3	-0.2
Balboa	1.4 ± 0.1	-0.1	-0.2	-0.1
Cristobal	1.4 ± 0.1	-0.1	-0.2	-0.1
Quequen	0.8 ± 0.2	-0.2	-0.5	-0.4
Buenos Aires	1.6 ± 0.2	-0.5	-0.7	-0.5
Honolulu	1.5 ± 0.1	-0.2	-0.2	-0.1

[a] Rates of local sea level computed following to Eq. (3.6).
[b] Local GIA correction computed following Eq. (3.18).

TGs, covering the surface of the ocean. As this is not the case, the GMSL rate can therefore be expressed as:

$$\mu' = g' \pm \mathrm{rms} \tag{3.23}$$

or

$$\mu' = g' \pm \mathrm{sdom} \quad . \tag{3.24}$$

Table 3.6: Rates of local sea level (before and after applying GIA-correction) for sites in the D97 set.

Region	TG site	$\rho^{(a)}$	$\rho'^{(b)}$		
			ICE-3G	ICE-5G	ICE-6G
		$(\mathrm{mm\,yr^{-1}})$	$(\mathrm{mm\,yr^{-1}})$	$(\mathrm{mm\,yr^{-1}})$	$(\mathrm{mm\,yr^{-1}})$
English Channel	Newlin	1.9 ± 0.1	1.8 ± 0.1	1.7 ± 0.1	1.7 ± 0.1
	Brest	1.0 ± 0.1	0.9 ± 0.1	0.8 ± 0.1	0.8 ± 0.1
Atlantic Ocean	Cascais	1.3 ± 0.1	1.5 ± 0.1	1.4 ± 0.1	1.3 ± 0.1
	Lagos	1.6 ± 0.2	1.7 ± 0.2	1.6 ± 0.2	1.6 ± 0.2
	Tenerife	1.6 ± 0.2	1.6 ± 0.2	1.6 ± 0.2	1.6 ± 0.2
Mediterranean	Marseille	1.3 ± 0.1	1.4 ± 0.1	1.3 ± 0.1	1.3 ± 0.1
Sea	Genova	1.2 ± 0.1	1.4 ± 0.1	1.2 ± 0.1	1.2 ± 0.1
	Trieste	1.4 ± 0.1	1.6 ± 0.1	1.4 ± 0.1	1.5 ± 0.1
New Zealand	Auckland II	1.3 ± 0.1	1.7 ± 0.2	1.6 ± 0.2	1.5 ± 0.1
	Wellington II	2.0 ± 0.2	2.5 ± 0.2	2.4 ± 0.2	2.3 ± 0.2
Pacific Ocean	Honolulu	1.5 ± 0.1	1.7 ± 0.1	1.7 ± 0.1	1.7 ± 0.1
North America	San Francisco	1.5 ± 0.1	1.6 ± 0.1	0.9 ± 0.1	0.9 ± 0.1
West Coast	Santa Monica	1.6 ± 0.1	1.9 ± 0.1	1.2 ± 0.1	1.1 ± 0.2
	La Jolla	2.0 ± 0.1	2.3 ± 0.1	1.7 ± 0.1	1.6 ± 0.1
	San Diego	2.2 ± 0.1	2.5 ± 0.1	1.9 ± 0.1	1.8 ± 0.1
Central America	Balboa	1.4 ± 0.1	1.6 ± 0.1	1.6 ± 0.1	1.6 ± 0.1
	Cristobal	1.4 ± 0.1	1.5 ± 0.1	1.6 ± 0.1	1.5 ± 0.1
South America	Quequen	0.8 ± 0.2	1.0 ± 0.2	1.4 ± 0.2	1.3 ± 0.2
	Buenos Aires	1.6 ± 0.2	2.0 ± 0.2	2.2 ± 0.2	2.1 ± 0.2
South East	Pensacola	2.5 ± 0.1	2.6 ± 0.1	1.9 ± 0.1	1.9 ± 0.1
North America	Key West	2.5 ± 0.1	2.6 ± 0.1	2.4 ± 0.1	2.2 ± 0.1
	Fernandina	2.2 ± 0.1	2.2 ± 0.1	1.6 ± 0.1	1.6 ± 0.1
μ $(\mathrm{mm\,yr^{-1}})^{(c)}$		(1.6 ± 0.5)	(1.8 ± 0.5)	(1.6 ± 0.4)	(1.6 ± 0.4)

[a] Uncorrected rates of local sea level computed following to Eq. (3.6).
[b] Corrected rates of local sea level computed following to Eq. (3.20).
[c] Uncorrected (column 3) and corrected (columns 4 to 6) estimates of GMSLR for the set considered, following Eqs. 3.11 and 3.23.

Table 3.7: Rates of local sea level (before and after applying GIA-correction) for sites in the SG01 set.

Region	TG site	$\rho^{(a)}$	$\rho'^{(b)}$		
			ICE-3G	ICE-5G	ICE-6G
		($\mathrm{mm\,yr^{-1}}$)	($\mathrm{mm\,yr^{-1}}$)	($\mathrm{mm\,yr^{-1}}$)	($\mathrm{mm\,yr^{-1}}$)
Siberia	Tiksi Bukhta	1.6 ± 0.2	1.5 ± 0.2	2.0 ± 0.2	1.8 ± 0.2
Northern Europe	Heimsjo	-1.2 ± 0.2	2.1 ± 0.4	1.8 ± 0.4	1.7 ± 0.4
	Smogen	-1.7 ± 0.1	0.9 ± 0.3	1.6 ± 0.3	1.3 ± 0.3
Scotland	Aberdeen II	0.6 ± 0.2	0.5 ± 0.2	1.0 ± 0.2	0.9 ± 0.2
	North Shield	1.9 ± 0.1	2.0 ± 0.1	2.2 ± 0.1	2.2 ± 0.1
English Channel	Newlin*	1.9 ± 0.1	1.8 ± 0.1	1.7 ± 0.1	1.7 ± 0.1
	Brest*	1.0 ± 0.1	0.9 ± 0.1	0.8 ± 0.1	0.8 ± 0.1
Atlantic Ocean	Lagos*	1.6 ± 0.2	1.7 ± 0.2	1.6 ± 0.2	1.6 ± 0.2
Mediterranean	Marseille*	1.3 ± 0.1	1.4 ± 0.1	1.3 ± 0.1	1.3 ± 0.1
Sea	Genova*	1.2 ± 0.1	1.4 ± 0.1	1.2 ± 0.1	1.2 ± 0.1
	Trieste*	1.4 ± 0.1	1.6 ± 0.1	1.4 ± 0.1	1.5 ± 0.1
	Bakar	1.1 ± 0.2	1.3 ± 0.2	1.1 ± 0.2	1.2 ± 0.2
Black Sea	Sevastopol	1.3 ± 0.2	1.1 ± 0.2	1.1 ± 0.2	1.1 ± 0.2
	Tuapse	2.4 ± 0.1	2.4 ± 0.1	2.3 ± 0.1	2.3 ± 0.1
Australia	Fremantle	1.7 ± 0.1	2.1 ± 0.1	2.0 ± 0.1	1.8 ± 0.1
New Zealand	Auckland II*	1.3 ± 0.1	1.7 ± 0.2	1.6 ± 0.2	1.5 ± 0.1
Central America	Balboa*	1.4 ± 0.1	1.6 ± 0.1	1.6 ± 0.1	1.6 ± 0.1
	Cristobal*	1.4 ± 0.1	1.5 ± 0.1	1.6 ± 0.1	1.5 ± 0.1
South America	Quequen*	0.8 ± 0.2	1.0 ± 0.2	1.4 ± 0.2	1.3 ± 0.2
	Buenos Aires*	1.6 ± 0.2	2.0 ± 0.2	2.2 ± 0.2	2.1 ± 0.2
Pacific Ocean	Honolulu*	1.5 ± 0.1	1.7 ± 0.1	1.7 ± 0.1	1.7 ± 0.1
μ ($\mathrm{mm\,yr^{-1}}$)$^{(c)}$		(1.2 ± 1.0)	(1.5 ± 0.5)	(1.6 ± 0.4)	(1.5 ± 0.4)

[a] Uncorrected rates of local sea level computed following to Eq. (3.6).
[b] Corrected rates of local sea level computed following to Eq. (3.20).
[c] Uncorrected (column 3) and corrected (columns 4 to 6) estimates of GMSLR for the set considered, following Eqs. 3.11 and 3.23.

Chapter 4

Results

4.1 Long-term GMSLR estimates

The various GMSLR estimates obtained for the three TG sets are summarized in Table 4.1. The resulting values of μ must be compared with an original estimate of $\mu = (1.8 \pm 0.1)\,\mathrm{mm\,yr^{-1}}$ (corrected for ICE-3G) for Douglas [1997] and an essentially set-independent and model-independent value of $\mu = (1.5 \pm 0.1)\,\mathrm{mm\,yr^{-1}}$ for Spada & Galassi [2012]. The uncertainty for both estimates is the standard deviation of the mean. Figures 4.1, 4.2 and 4.3 show the histograms of the distribution of the rates of sea level r_k for each combination of set and GIA correction.

The results showed in Table 4.1 point to a GMSLR value of 1.5 ÷ 1.6 mm yr^{-1}, with the noticeable exception of the D97 set for the ICE-3G correction (estimate number 3 in Table 4.1). For the reasons already discussed, its very high value of 1.8 ± 0.5 mm yr^{-1} is not confirmed for the other two models and is resolved for the D97R set, confirming the conclusions of Spada & Galassi [2012]. The inclusions of sites covered by ice during the LGM (see criterion (V) in Table 2.1) in the SG01 set increases the spread of individual rates, resulting in a lower average associated to a quite large error (comparable to the value of the estimate itself), which is corrected by applying a GIA correction.

Table 4.1: Estimates of secular GMSLR ($\mu' = g' \pm \text{rms}$) obtained, corresponding to different subsets of TGs and GIA corrections. The statistics wrms and sdom are also shown

TG set		$\mu = g \pm \text{rms}$ (mm yr^{-1})	wrms (mm yr^{-1})	sdom (mm yr^{-1})	GIA correction
1	D97	1.6 ± 0.5	0.5	0.1	No
2	D97	1.8 ± 0.5	0.6	0.1	ICE-3G
3	D97	1.6 ± 0.4	0.4	0.1	ICE-5G
4	D97	1.6 ± 0.4	0.4	0.1	ICE-6G
5	D97R	1.4 ± 0.3	0.3	0.1	No
6	D97R	1.6 ± 0.4	0.4	0.1	ICE-3G
7	D97R	1.6 ± 0.4	0.4	0.1	ICE-5G
8	D97R	1.5 ± 0.4	0.4	0.1	ICE-6G
9	SG01	1.2 ± 1.0	0.9	0.2	No
10	SG01	1.5 ± 0.5	0.4	0.1	ICE-3G
11	SG01	1.6 ± 0.4	0.5	0.1	ICE-5G
12	SG01	1.5 ± 0.4	0.4	0.1	ICE-6G

Douglas [1997] computed regional averages as an intermediate step. This has been inspected for every estimate in Table 4.1, but did not produce significant changes at the $0.1\,\text{mm yr}^{-1}$ level. The effect of the rotational feedback on the sea level, which has been considered in a run of SELEN with the same parameters as ICE-6G, similarly produced small changes to the estimates and their uncertainty.

The long-term GMSLR estimate of $\mu = (1.5 \pm 0.1)\,\text{mm yr}^{-1}$ from Spada & Galassi [2012] is therefore confirmed and updated with a new ice model and up-to-date data.

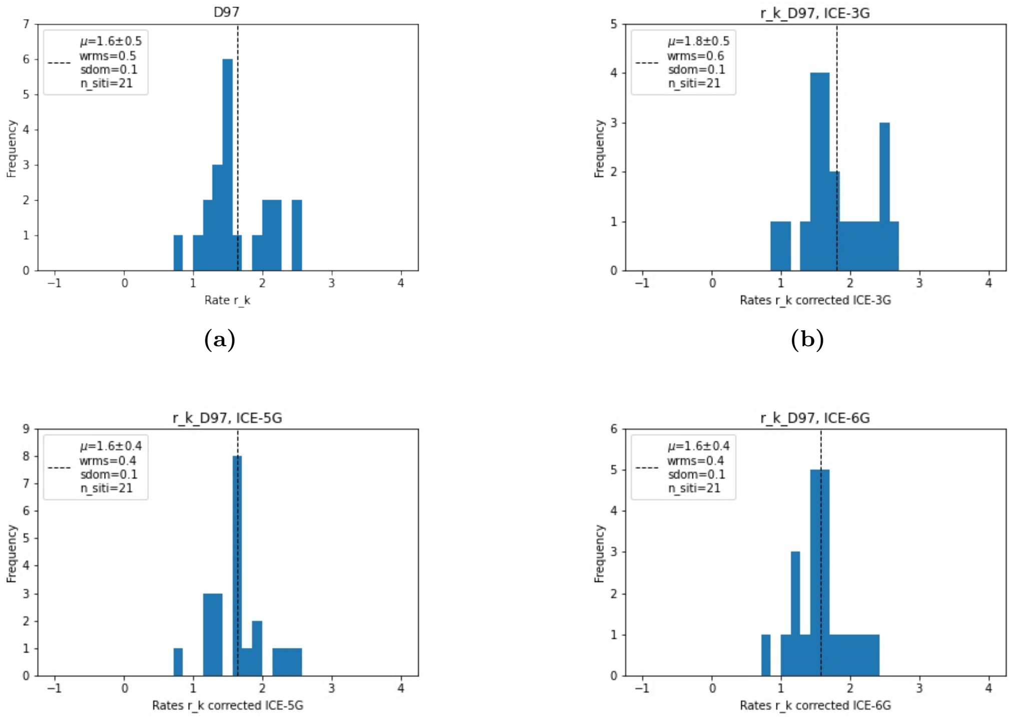

(a) **(b)** **(c)** **(d)**

Figure 4.1: Distribution of local sea level rates for the D97 set. Values of μ are computed following Equation (3.11). A vertical dashed line marks the value of μ. (a) uncorrected (b) corrected for ICE-3G (c) corrected for ICE-5G (d) corrected for ICE-6G.

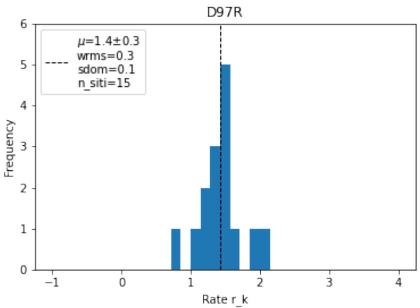

(a)

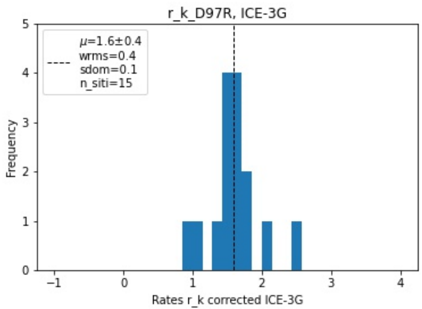

(b)

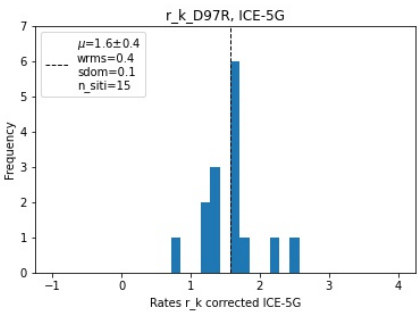

(c)

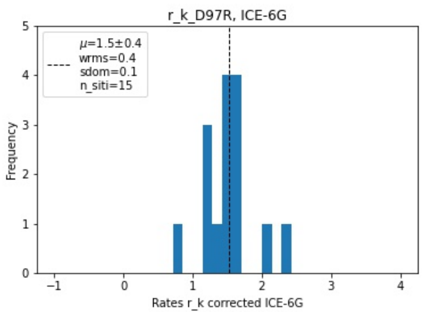

(d)

Figure 4.2: Distribution of local sea level rates for the D97R set. Values of μ are computed following Equation (3.11). A vertical dashed line marks the value of μ. (a) uncorrected (b) corrected for ICE-3G (c) corrected for ICE-5G (d) corrected for ICE-6G.

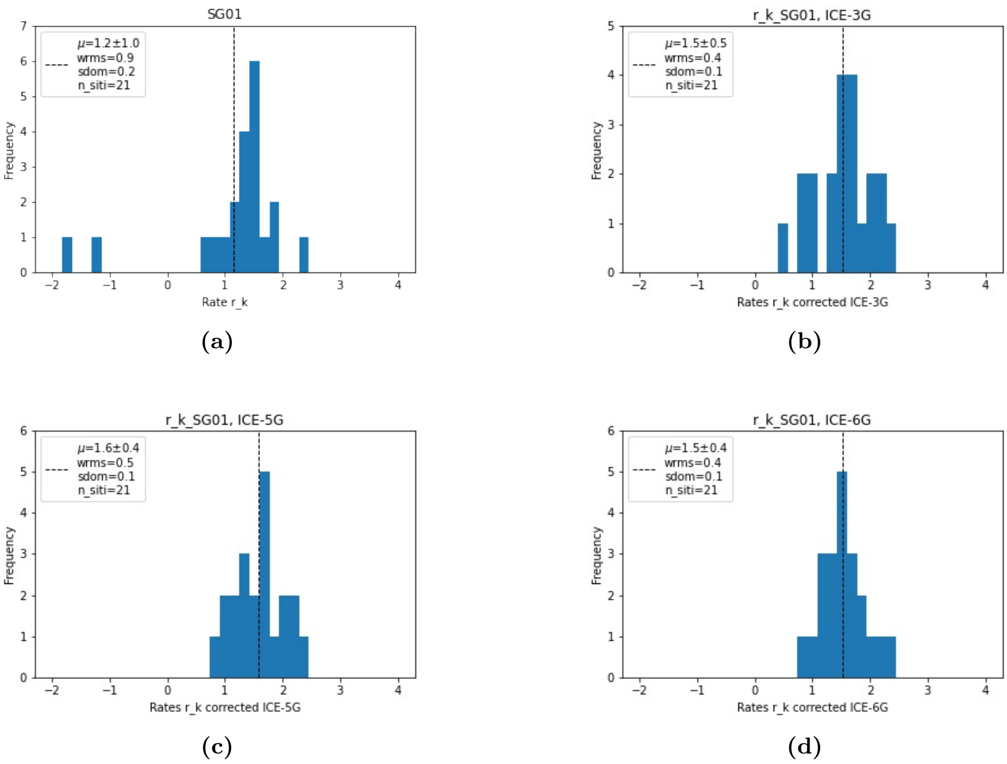

(a) **(b)** **(c)** **(d)**

Figure 4.3: Distribution of local sea level rates for the SG01 set. Values of μ are computed following Equation (3.11). A vertical dashed line marks the value of μ. (a) uncorrected (b) corrected for ICE-3G (c) corrected for ICE-5G (d) corrected for ICE-6G.

4.2 Contemporary GMSLR estimates

As mentioned in Chapter 3, the GMSLR has been assumed to be constant. This allows for relatively simple statistics, without the more complex approaches that would be necessary to attempt to discern a true acceleration from the characteristic oscillations that characterize the sea level. However, estimates of the altimetry-based contemporary GMSLR from Cazenave *et al.* [2018] provide a much higher value of $\mu = (3.1 \pm 0.3)\,\mathrm{mm\,yr^{-1}}$, with an acceleration of $0.1\,\mathrm{mm\,yr^{-2}}$. According to these authors, estimates from gravimetric missions close the sea level budget to within $0.3\,\mathrm{mm\,yr^{-1}}$, hinting that the high value of μ over the 25 years considered is a real signal.

The first logical step to cover the gap between TGs and satellite data is to use the former to estimate GMSLR for the same period and compare the two results. As discussed in Section 2.2, the TG sets considered above are not suitable for estimates over short periods of time, as they simply do not contain enough data to produce significant results. As the need for a trade-off between the length of the record and the spatial coverage of the sea is not valid in this case, a preliminary investigation can be carried out by maximizing the spatial coverage, *i.e.*, considering the whole TG record for this time period.

Three different sets will be evaluated, based on the timespan considered: the first (the "ALL" set) consists of the entire RLR dataset, the second (the "secular" dataset) consists of records from the year 1900 to the year 2000, the third (the "contemporary" set) consists of records from the year 1993 to the present day, and will be compared to the result of Cazenave *et al.* [2018]. Two requirements will be applied to the series: the first is that each record must contain at least three valid yearly observations over the timespan considered, for consistency with Equation (3.4), the second is that a minimum completeness of $C_k > 70\%$ (computed following Equation 2.1) is met. The resulting sets consist of 1278, 1045 and 875 TGs for the "ALL", "secular" and "contemporary" set, respectively. The same statistics and

Table 4.2: Estimates of GMSLR ($\mu' = g' \pm \mathrm{sdom}$) obtained, corresponding to different subsets of TGs and GIA corrections. The three sets considered have a completeness (computed following Eq. 2.1) $C_k > 70\%$ and differ in the time span considered. The statistics rms and wrms are also shown. N_{TG} is the number of TGs in the set.

TG set		N_{TG}	$\mu' = g' \pm \mathrm{sdom}$ ($\mathrm{mm\,yr^{-1}}$)	rms (wrms) ($\mathrm{mm\,yr^{-1}}$)	GIA correction
1	ALL	1278	1.8 ± 0.2	6.0 (6.3)	No
2	ALL		2.2 ± 0.2	5.8 (5.4)	ICE-3G
3	ALL		2.3 ± 0.2	5.8 (6.0)	ICE-5G
4	ALL		2.2 ± 0.2	5.8 (5.5)	ICE-6G
5	Secular	1045	2.0 ± 0.3	8.2 (7.1)	No
6	Secular		2.4 ± 0.2	8.0 (6.7)	ICE-3G
7	Secular		2.6 ± 0.2	8.0 (7.0)	ICE-5G
8	Secular		2.5 ± 0.2	8.0 (6.6)	ICE-6G
9	Contemporary	875	3.1 ± 0.2	6.5 (7.3)	No
10	Contemporary		3.4 ± 0.2	6.4 (6.8)	ICE-3G
11	Contemporary		3.5 ± 0.2	6.4 (7.2)	ICE-5G
12	Contemporary		3.4 ± 0.2	6.4 (7.0)	ICE-6G

corrections considered in Chapter 3 will be applied to three sets.

The distributions of rates ρ_k for the different combinations of sets and GIA models are reported in Figures 4.4, 4.5 and 4.6, respectively. Since the number of TGs is so high, the deviations of local rates from their average can, to a first approximation, be viewed as random noise, making the standard deviation of the mean the most appropriate choice for the evaluation of the uncertainty of μ. As a consequence, the GMSLR estimate will thus be expressed as $\mu = g' \pm \mathrm{sdom}$.

The resulting GMSLR estimates are reported in Table 4.2. GIA corrected rates are in broad agreement for each of the three sets considered. This hints that with such a high number of sites considered, the differences between the three GIA models employed do not produce substantial differences on the global average. The estimates for the two longer periods (from the "ALL" and "secular" sets) produce higher results than achieved from the long records previously considered, exceeding them by $0.7 \div 1.1$ mm yr^{-1}. This is likely a consequence of the inclusion of sites as short as three years. Further analysis should apply corrections at higher frequencies, considered negligible in the above, such as the effect of atmospheric pressure. Additionally, in this preliminary estimate each site has the same weight on the average, regardless of his length. The implementation in the average of a weight function based on the individual record length would better constrain these estimates.

Estimates from the "contemporary" set give a value of $\mu = 3.4 \div 3.5 \pm 0.2\ \mathrm{mm\,yr^{-1}}$. This result does not contradict the altimetry estimate of $\mu = (3.1 \pm 0.3)\,\mathrm{mm\,yr^{-1}}$ from Cazenave *et al.* [2018], with the two rates overlapping. The better performance of this approach for shorter periods of time reflects the better spatial sampling achieved at any time in the frame considered, although corrections for effects on shorter periods (*e.g.*, the inverse barometer effect) should be further explored.

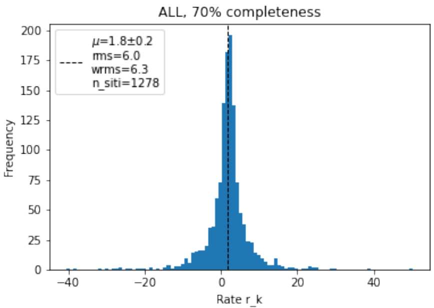

(a)

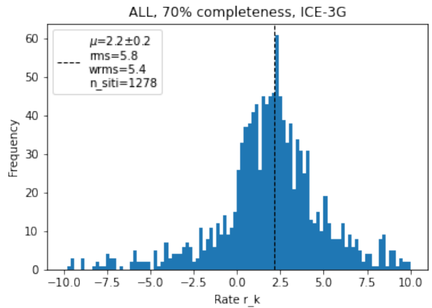

(b)

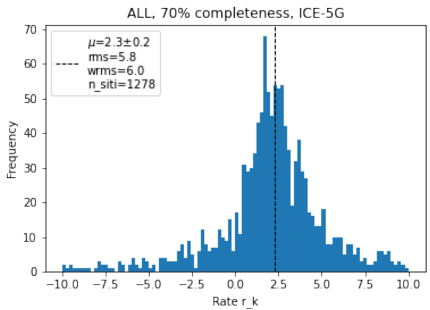

(c)

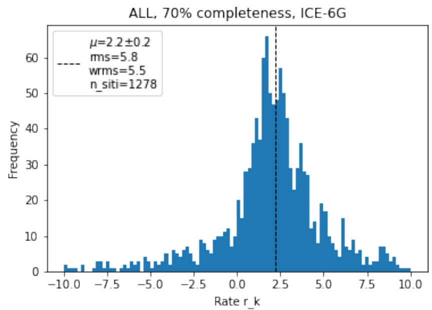

(d)

Figure 4.4: Distribution of local sea level rates for the ALL set. Values of μ are computed following Equation (3.12). A vertical dashed line marks the value of μ. (a) uncorrected (b) corrected for ICE-3G (c) corrected for ICE-5G (d) corrected for ICE-6G.

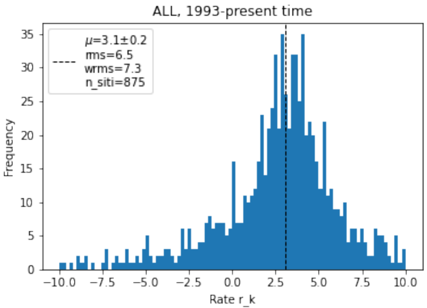

(a)

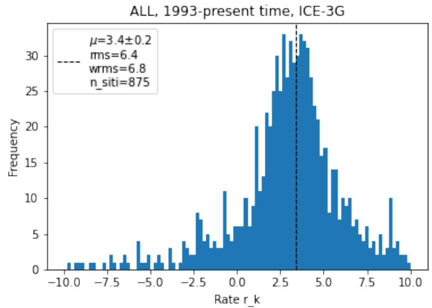

(b)

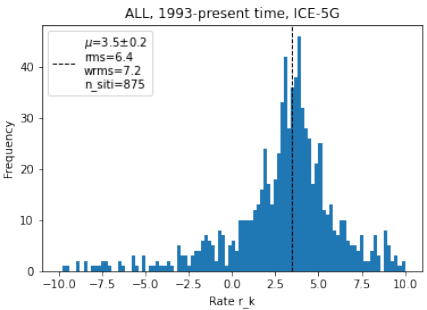

(c)

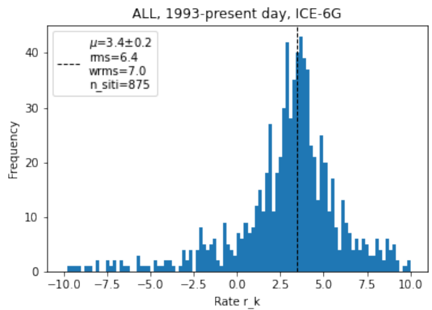

(d)

Figure 4.5: Distribution of local sea level rates for the contemporary set. Values of μ are computed following Equation (refMuSDOM). A vertical dashed line marks the value of μ. (a) uncorrected (b) corrected for ICE-3G (c) corrected for ICE-5G (d) corrected for ICE-6G.

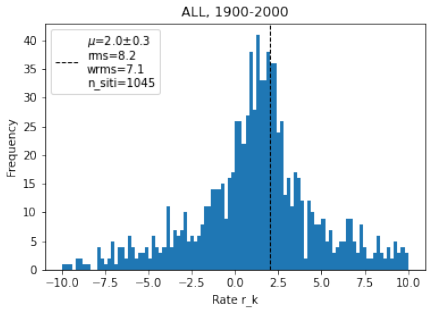

(a)

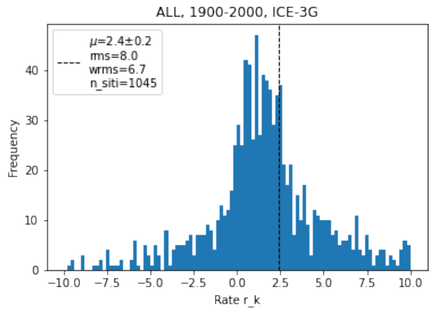

(b)

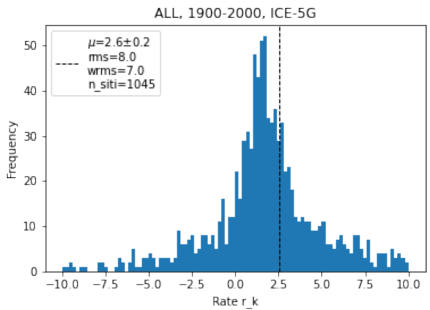

(c)

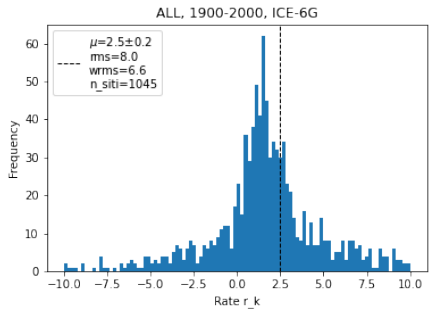

(d)

Figure 4.6: Distribution of local sea level rates for the secular set. Values of μ are computed following Equation (3.12). A vertical dashed line marks the value of μ. (a) uncorrected (b) corrected for ICE-3G (c) corrected for ICE-5G (d) corrected for ICE-6G.

Chapter 5

Conclusions and final remarks

The estimates of long term (secular) global mean sea-level rise from Douglas [1997] and Spada & Galassi [2012] were tested under a new iteration of the GIA model originally used (ICE-3G, Tushingham & Peltier [1991]) and updated in view of the evolution of the TG record. The resulting estimate of $(1.5 \pm 0.4)\,\mathrm{mm\,yr^{-1}}$ essentially confirmed the results of Spada & Galassi [2012]. The issues they found in the choice of the dataset in Douglas [1997] were also confirmed.

Finally, the entire TG dataset was used to estimate the contemporary (*i.e.*, post 1993) value of GMSLR, giving a value compatible with altimetry observations from Cazenave *et al.* [2018]. Applying the same methods to a longer period of time (either the entire record or limited to the twentieth century) provided estimates which exceed the value given above by $0.7 \div 1.1$ mm yr^{-1}. This discrepancy is likely due to the poor sampling of high-period sea-level anomalies related to changes in atmospheric systems over the oceans. As discussed in Chapter 2 the choice of the TG set is a trade-off between the geographical distribution and the length and quality of the records. In this case, records as short as three years were considered to have the same weight in view of the relatively short time period considered. In order to use this kind of set for longer periods, a weight based on the record lengths should be introduced, as well as the use of regional averages as an intermediate step. The good agreement of results under different GIA models (with differences not exceeding $\sim 10\%$ of the GMSLR estimates, comparable to the differences found using the D97 and SG01 set) suggests that the choice of the GIA model plays a minor role in this discrepancy.

When local rates of sea-level change were computed in Equation (3.20), no additional uncertainty due to the GIA model was computed. Due to the implicit nature of the SLE, the best way to account for possible errors in the GIA modelling is to combine different models and compare them using a probabilistic method. Several approaches have been used in the last decade: Hay *et al.* [2015] and Dangendorf *et al.* [2019] used an algorithmic approach using a Kalman Smoother, Melini & Spada [2019] used a Monte Carlo simulation to compare models with modified parameters, Spada & Melini [2022] used an ensemble approach. In any case, even though the consequences on local rates can be quite important, when averaging to obtain the GMSLR the effect of GIA corrections is probably at least one order of magnitude lower than the formal errors computed. The ensemble approach used in Spada & Melini [2022], when applied to the sites in SG01, reached the same conclusions.

In Chapter 3 two different estimates of the error were introduced, with the root mean square (rms) for estimates from the smaller sets and the standard deviation of the mean (sdom) for estimates from the larger sets. The latter is based on the assumption that the local rates are randomly distributed around their average. This ultimately means that the deviations of the individual rates from the global mean can be treated as random noise, and the Central Limit Theorem can be applied. This is formally not true. However, in view of the very high number of sites ($N_{TG} > 800$) considered when the sdom is used, as an approximation the distribution is considered to be random.

Likewise, any temporal correlation of sea-level variation was ignored, *i.e.*, each annual observation was considered to be independent of previous years. It is well established that not only sea level, but also several other physical quantities associated to it, such as ocean surface temperature and sea-level pressure exhibit temporally correlated noise. Bos *et al.* [2014] applied several autoregressive models to TG and satellite GMSLR estimates and found that neglecting this aspect normally does not change the rate estimate, although it may cause an underestimation of the uncertainty.

Looking at Figure 2.3 it is clear that the Southern Emisphere, and especially Africa are heavily under-represented. In the first part of this work, the poor distribution of TGs was mitigated by the high quality and length of the TGs considered. This is not true for the estimates in Table 4.2. As discussed in Section 2.3, sea-level changes are not uniform over the globe, with meridional differences largely attributable to the not uniform heating of the ocean surface and to gravitational changes due to contemporary ice melting, which is limited in the Southern Emisphere (Cazenave *et al.* [2018]). There are methods (*e.g.*, Empirical Orthogonal Functions) used to project spatial patterns of sea level change in the past, allowing to mitigate the effects of the poor distribution of TGs.

As discussed in Section 2.3 the lack of coverage in the TG record for open ocean raises the question of how well they represent the behaviour of the entire ocean. There are at least two main phenomena that could raise problems. The first is the Ekman dynamic, both nearshore (due to coastal upwelling/downwelling in the presence of longshore winds) and on open oceans (Ekman pumping/suction near the equator). The second is related to shifts in the oscillating patterns of atmospheric pressure centers on the open ocean, as they are related to changes in sea surface temperature, salinity and pressure. Kolker & Hameed [2007] found the sea level in several sites in the Northern Atlantic to be correlated to the position and intensity of the Azores High and the Icelandic Low pressure systems. According to their estimates, GMSLR could potentially be overestimated by several tenths of millimetre.

Given the quite simple statistical approach herein used, only the average sea level trend was computed. An estimate of sea-level acceleration would require a much more refined theory, and is subject to several problems. Palmer *et al.* [2021] employed an unweighted quadratic fit obtaining an acceleration of $0.0053\,\mathrm{mm\,yr^{-2}}$ over the 20^{th} century. The relative shortness of the instrumental record , together with its uneven sampling of the sea surface, makes it extremely difficult to assess whether this apparent acceleration is real, or is just part of a low frequency oscillation or an artefact of the TG set considered. As a matter of fact, oscillations with a characteristic period of up to 64 years related to mass movements in the core of the Earth have been observed by Ding *et al.* [2021], and would need an extremely long record to be resolved with a simple quadratic fit. It is virtually certain, however, that the contemporary acceleration of $1\,\mathrm{mm\,yr^{-2}}$ observed by satellite altimetry (see Cazenave *et al.* [2018]) is unprecedented in the last millennia (see the IPCC Sixth Assessment Report, Gulev *et al.* [2021]).

Some of the maps in this work have been drawn using PyGMT (Uieda *et al.* [2021]), a Python interface for the Generic Mapping Tool public domain software of Wessel *et al.* [2019].

Bibliography

Anthoff, D, Nicholls, RJ, & Tol, RSJ. 2010. The economic impact of substantial sea-level rise. *Mitigation and Adaptation Strategies for Global Change*, **15**(4), 321–335.

Bamber, JL, Westaway, RM, Marzeion, B, & Wouters, B. 2018. The land ice contribution to sea level during the satellite era. *Environmental Research Letters*, **13**(6), 063008.

Barnett, TP. 1983. Recent changes in sea level and their possible causes. *Climatic change*, **5**(1), 15–38.

Barnett, TP. 1984. The estimation of 'global' sea level change: a problem of uniqueness. *Journal of Geophysal Research*, **89**(C5), 7980–7988.

Benjamin, J, Rovere, A, Fontana, A, Furlani, S, Vacchi, M, Inglis, R H, Galili, E, Antonioli, F, Sivan, D, Miko, S, *et al.* 2017. Late Quaternary sea-level changes and early human societies in the central and eastern Mediterranean Basin: An interdisciplinary review. *Quaternary International*, **449**, 29–57.

Bos, MS, Williams, SDP, Araújo, IB, & Bastos, L. 2014. The effect of temporal correlated noise on the sea level rate and acceleration uncertainty. *Geophysical Journal International*, **196**(3), 1423–1430.

Cabanes, C, Cazenave, A, & Le Provost, C. 2001. Sea level rise during past 40 years determined from satellite and in situ observations. *Science*, **294**(5543), 840–842.

Cailleux, A. 1952. Récentes variations du niveau des mers et des terres. *Bulletin de la Société Géologique de France*, **6**(1-3), 135–144.

Carbognin, L, Teatini, P, & Tosi, L. 2004. Eustacy and land subsidence in the Venice Lagoon at the beginning of the new millennium. *Journal of Marine Systems*, **51**(1-4), 345–353.

Cazenave, A, & Nerem, RS. 2004. Present-day sea level change: Observations and causes. *Reviews of Geophysics*, **42**(3).

Cazenave, A, Meyssignac, B, Ablain, M, Balmaseda, M, Bamber, J, Barletta, V, Beckley, B, Benveniste, J, Berthier, E, Blazquez, A, *et al.* 2018. Global sea-level budget 1993-present. *Earth System Science Data*, **10**(3), 1551–1590.

Church, JA, & White, NJ. 2006. A 20th century acceleration in global sea-level rise. *Geophysical Research Letters*, **33**(1), L01602.

Church, JA, & White, NJ. 2011. Sea-level rise from the late 19th to the early 21st century. *Surveys in Geophysics*, **32**(4-5), 585–602.

Church, JA, Gregory, JM, Huybrechts, P, Kuhn, M, Lambeck, K, Nhuan, MT, Qin, D, & Woodworth, PL. 2001. Climate Change 2001: The Scientific Basis: Contribution of Working Group I to the Third Assessment Report of the Intergovernmental Panel. *Pages 639–694 of:* Houghton, JT, Ding, Y, Griggs, DJ, Noguer, M., Van der Linden, PJ, Dai, X, Maskell, K, & CA, Johnson (eds), *Changes in sea level.* Cambridge University Press, Cambridge.

Church, JA, White, NJ, Coleman, R, Lambeck, K, & Mitrovica, JX. 2004. Estimates of the regional distribution of sea level rise over the 1950-2000 period. *Journal of climate*, **17**(13), 2609–2625.

Dangendorf, S, Marcos, M, Wöppelmann, G, Conrad, CP, Frederikse, T, & Riva, R. 2017. Reassessment of 20th century global mean sea level rise. *Proceedings of the National Academy of Sciences*, **114**(23), 5946–5951.

Dangendorf, S, Hay, C, Calafat, FM, Marcos, M, Piecuch, CG, Berk, K, & Jensen, J. 2019. Persistent acceleration in global sea-level rise since the 1960s. *Nature Climate Change*, **9**(9), 705–710.

Davis, JL, & Mitrovica, JX. 1996. Glacial isostatic adjustment and the anomalous tide gauge record of eastern North America. *Nature*, **379**, 331–333.

Ding, H, Jin, T, Li, J, & Jiang, W. 2021. The Contribution of a Newly Unraveled 64 Years Common Oscillation on the Estimate of Present-Day Global Mean Sea Level Rise. *Journal of Geophysical Research: Solid Earth*, **126**(8), e2021JB022147.

Douglas, BC. 1991. Global sea level rise. *Journal of Geophysical Research Oceans (1978-2012)*, **96**(C4), 6981–6992.

Douglas, BC. 1997. Global sea leve rise: a redetermination. *Surveys in Geophysics*, **18**, 279–292.

Emery, KO. 1980. Relative sea levels from tide-gauge records. *Proceedings of the National Academy of Sciences*, **77**(12), 6968–6972.

Emery, KO, Aubrey, DG, & Jansa, L. 1991. *Sea levels, land levels, and tide gauges*. Vol. 237. Springer-Verlag New York.

Fairbridge, RW, & Krebs Jr, OA. 1962. Sea level and the southern oscillation. *Geophys. J. Int.*, **6**(4), 532–545.

Farrell, WE, & Clark, James A. 1976. On postglacial sea level. *Geophysical Journal International*, **46**(3), 647–667.

Frederikse, T, Jevrejeva, S, Riva, REM, & Dangendorf, S. 2018. A consistent sea-level reconstruction and its budget on basin and global scales over 1958-2014. *Journal of Climate*, **31**(3), 1267–1280.

Frederikse, T, Landerer, F, Caron, L, Adhikari, S, Parkes, D, Humphrey, VW, Dangendorf, S, Hogarth, P, Zanna, L, Cheng, L, *et al.* 2020. The causes of sea-level rise since 1900. *Nature*, **584**(7821), 393–397.

Gehrels, R. 2010. Sea-level changes since the Last Glacial Maximum: an appraisal of the IPCC Fourth Assessment Report. *Journal of Quaternary Science*, **25**(1), 26–38.

Gornitz, V, & Lebedeff, S. 1987. Global sea-level changes during the past century.

Gornitz, V, Lebedeff, S, & Hansen, JE. 1982. Global sea level trend in the past century. *Science*, **215**(4540), 1611–1614.

Gröger, M, & Plag, HP. 1993. Estimations of a global sea level trend: limitations from the structure of the PSMSL global sea level data set. *Global and Planetary Change*, **8**(3), 161–179.

Gulev, SK, Thorne, PW, Ahn, J, Dentener, FJ, Domingues, CM, Gerland, S, Gong, D, Kaufman, DS, Nnamchi, HC, Quaas, J, Rivera, JA, Sathyendranath, S, Smith, SL, Trewin, B, von Schuckmann, K, & Vose, RS. 2021. *Changing State of the Climate System*. Cambridge, United Kingdom and New York, NY, USA: Cambridge University Press. Book Section 2.

Gutenberg, B. 1941. Changes in sea level, postglacial uplift, and mobility of the earth's interior. *Bulletin of the Geological Society of America*, **52**(5), 721–772.

Hagedoorn, JM, Wolf, D, & Martinec, Z. 2007. An estimate of global mean sea-level rise inferred from tide-gauge measurements using glacial-isostatic models consistent with the relative sea-level record. *Pure and Applied Geophysics*, **164**(4), 791–818.

Hamlington, BD, Leben, RR, Nerem, RS, Han, W, & Kim, K-Y. 2011. Reconstructing sea level using cyclostationary empirical orthogonal functions. *Journal of Geophysical Research: Oceans*, **116**(C12).

Hannah, J. 2004. An updated analysis of long-term sea level change in New Zealand. *Geophysical Research Letters*, **31**(3).

Hay, CC, Morrow, E, Kopp, RE, & Mitrovica, JX. 2015. Probabilistic reanalysis of twentieth-century sea-level rise. *Nature*, **517**(7535), 481–484.

Holgate, SJ. 2007. On the decadal rates of sea level change during the twentieth century. *Geophysical research letters*, **34**(1).

Holgate, SJ, & Woodworth, PL. 2004. Evidence for enhanced coastal sea level rise during the 1990s. *Geophysical Research Letters*, **31**(7).

Holgate, SJ, Matthews, A, Woodworth, PL, Rickards, LJ, Tamisiea, ME, Bradshaw, E, Foden, PR, Gordon, KM, Jevrejeva, S, & Pugh, J. 2013. New data systems and products at the permanent service for mean sea level. *Journal of Coastal Research*, **29**(3), 493–504.

Jevrejeva, S, Moore, JC, Grinsted, A, Matthews, AP, & Spada, G. 2014. Trends and acceleration in global and regional sea levels since 1807. *Global and Planetary Change*, **113**, 11–22.

Kalinin, GP, & Klige, RK. 1978. Variation in the world sea level. *World Water Balance and Water Resources of the Earth*, 581–585.

Kolker, AS, & Hameed, S. 2007. Meteorologically driven trends in sea level rise. *Geophysical Research Letters*, **34**(23).

Lambeck, K, Smither, C, & Johnston, P. 1998. Sea-level change, glacial rebound and mantle viscosity for northern Europe. *Geophysical Journal International*, **134**(1), 102–144.

Lambeck, K, Rouby, H, Purcell, A, Sun, Y, & Sambridge, M. 2014. Sea level and global ice volumes from the Last Glacial Maximum to the Holocene. *Proceedings of the National Academy of Sciences*, **111**(43), 15296–15303.

Levitus, S, Antonov, JI, Boyer, TP, Baranova, OK, Garcia, HE, Locarnini, RA, Mishonov, AV, Reagan, JR, Seidov, D, Yarosh, ES, *et al.* 2012. World ocean heat content and thermosteric sea level change (0-2000 m), 1955-2010. *Geophysical Research Letters*, **39**(10).

Lisitzin, E. 1958. Le niveau moyen de la mer. *Bull3tin Informatif Comité Central d'Océanographie et d'Etude des Côtes (COEC)*, **10**, 254–262.

Lisitzin, E. 1974. *Sea-level changes*. Vol. 8. Elsevier Science.

Melini, D, & Spada, G. 2019. Some remarks on Glacial Isostatic Adjustment modelling uncertainties. *Geophysical Journal International*, **218**(1), 401–413.

Meyssignac, B, Becker, M, Llovel, W, & Cazenave, A. 2012. An assessment of two-dimensional past sea level reconstructions over 1950-2009 based on tide-gauge data and different input sea level grids. *Surveys in Geophysics*, **33**(5), 945–972.

Mitrovica, JX, & Davis, JL. 1995. Present-day post-glacial sea level change far from the Late Pleistocene ice sheets: Implications for recent analyses of tide gauge records. *Geophysical Research Letters*, **22**(18), 2529–2532.

Mitrovica, JX, Tamisiea, ME, Davis, JL, & Milne, GA. 2001. Recent mass balance of polar ice sheets inferred from patterns of global sea-level change. *Nature*, **409**(6823), 1026–1029.

Nakada, M, & Inoue, H. 2005. Rates and causes of recent global sea-level rise inferred from long tide gauge data records. *Quaternary Science Reviews*, **24**(10-11), 1217–1222.

Nakiboglu, SM, & Lambeck, K. 1991. Secular sea level change. *Pages 237–258 of:* Sabadini, R., Lambeck, K., & Boschi, E. (eds), *Glacial Isostasy, Sea Level and Mantle Rheology*. Kluwer Academic Publ.

Nerem, RS, & Mitchum, GT. 2001. Sea level change. *Pages 329–xxiii of: International Geophysics*, vol. 69. Elsevier.

Palmer, MD, Domingues, CM, Slangen, ABA, & Dias, FB. 2021. An ensemble approach to quantify global mean sea-level rise over the 20th century from tide gauge reconstructions. *Environmental Research Letters*, **16**(4), 044043.

Peltier, WR. 1986. Deglaciation-induced vertical motion of the North American continent and transient lower mantle rheology. *Journal of Geophysical Research: Solid Earth*, **91**(B9), 9099–9123.

Peltier, WR. 1996. Global sea level rise and glacial isostatic adjustment: an analysis of data from the east coast of North America. *Geophysical Research Letters*, **23**(7), 717–720.

Peltier, WR. 2001. Global glacial isostatic adjustment and modern instrumental records of relative sea level history. *Pages 65–95 of: International geophysics*, vol. 75. Elsevier.

Peltier, WR. 2004. Global glacial isostasy and the surface of the ice-age Earth: the ICE-5G (VM2) model and GRACE. *Annual Review of Earth and Planetary Sciences*, **32**, 111–149.

Peltier, WR, & Jiang, X. 1996. Mantle viscosity from the simultaneous inversion of multiple data sets pertaining to postglacial rebound. *Geophysical Research Letters*, **23**(5), 503–506.

Peltier, WR, & Tushingham, AM. 1989. Global sea level rise and the greenhouse effect: might they be connected? *Science*, **244**(4906), 806–810.

Peltier, WR, Argus, DF, & Drummond, R. 2015. Space geodesy constrains ice age terminal deglaciation: The global ICE-6G_C (VM5a) model. *Journal of Geophysical Research: Solid Earth*, **120**(1), 450–487.

Pirazzoli, PA. 1986. *Secular trends of relative sea-level (RSL) changes indicated by tide-gauge records*. Tech. rept. CNRS-INTERGEO, 191 Rue Saint Jacques, 75005 Paris, France.

Polli, S. 1952. Gli attuali movimenti verticali delle coste continentali. *Annals of Geophysics*, **5**(4), 597–602.

Ponte, RM. 2006. Low-frequency sea level variability and the inverted barometer effect. *Journal of Atmospheric and Oceanic Technology*, **23**(4), 619–629.

PSMSL. 2021. *Permanent Service for Mean Sea Level, Tide Gauge data. http://www.psmsl.org/obtaining.* [Online; retrieved 03-May-2021].

Ray, RD, & Douglas, BC. 2011. Experiments in reconstructing twentieth-century sea levels. *Progress in Oceanography*, **91**(4), 496–515.

Schubert, G, Turcotte, DL, & Olson, P. 2001. *Mantle convection in the Earth and planets.* Cambridge University Press.

Shennan, I, & Woodworth, PL. 1992. A comparison of late Holocene and twentieth-century sea-level trends from the UK and North Sea region. *Geophysical Journal International*, **109**(1), 96–105.

Spada, G, & Galassi, G. 2012. New estimates of secular sea level rise from tide gauge data and GIA modelling. *Geophysical Journal International*, **191**(3), 1067–1094.

Spada, G, & Melini, D. 2019. SELEN 4 (SELEN version 4.0): a Fortran program for solving the gravitationally and topographically self-consistent sea-level equation in glacial isostatic adjustment modeling. *Geoscientific Model Development*, **12**(12), 5055–5075.

Spada, G, & Melini, D. 2022. New estimates of ongoing sea level change and land movements caused by Glacial Isostatic Adjustment in the Mediterranean region. *Geophysical Journal International*, **229**(2), 984–998.

Spada, G, & Stocchi, P. 2006. *The sea level equation, theory and numerical examples.* Aracne Editrice.

Stewart, RW. 1989. Sea-level rise or coastal subsidence? *Atmosphere-Ocean*, **27**(3), 461–477.

Sturges, W, & Douglas, BC. 2011. Wind effects on estimates of sea level rise. *Journal of Geophysical Research: Oceans*, **116**(C6).

Sturges, W, & Hong, BG. 2001. Decadal variability of sea level. *Pages 165–180 of:* Douglas, BC, Kearney, MS, & Leatherman, SP (eds), *Sea level rise: History and consequences.* International Geophysics Series (75).

Tamisiea, ME. 2011. Ongoing glacial isostatic contributions to observations of sea level change. *Geophysical Journal International*, **186**(3), 1036–1044.

Taylor, JR. 1997. *An introduction to error analysis: the study of uncertainties in physical measurements.* University Science Books.

Tegmark, M. 1996. An icosahedron-based method for pixelizing the celestial sphere. *The Astrophysical Journal*, **470**(2), L81.

Trupin, A, & Wahr, J. 1990. Spectroscopic analysis of global tide gauge sea level data. *Geophysical Journal International*, **100**(3), 441–453.

Tushingham, AM, & Peltier, WR. 1991. ICE-3G - A new global model of late Pleistocene deglaciation based upon geophysical predictions of post-glacial relative sea level change. *Journal of Geophysical Research*, **96**(B3), 4497–4523.

Uieda, L, Tian, D, Leong, WJ, Schlitzer, W, Toney, L, Grund, M, Jones, M, Yao, J, Materna, K, Newton, T, Anant, A, Ziebarth, M, & Wessel, P. 2021 (June). *PyGMT: A Python interface for the Generic Mapping Tools.*

Unal, YS, & Ghil, M. 1995. Interannual and interdecadal oscillation patterns in sea level. *Climate Dynamics*, **11**(5), 255–278.

Valentin, H. 1954. *Die Kusten der Erde: Beitrage zur allgemeinen und regionalen Kustenmorphologie.* Geograph. Kartograph. Anst.

Wenzel, M, & Schröter, J. 2010. Reconstruction of regional mean sea level anomalies from tide gauges using neural networks. *Journal of Geophysal Research*, **115**(C8).

Wessel, P, Luis, JF, Uieda, L, Scharroo, R, Wobbe, F, Smith, WHF, & Tian, D. 2019. The generic mapping tools version 6. *Geochemistry, Geophysics, Geosystems*, **20**(11), 5556–5564.

Woodworth, PL. 2006. Some important issues to do with long-term sea level change. *Philosophical Transactions of the Royal Society A: Mathematical, Physical and Engineering Sciences*, **364**(1841), 787–803.

Woodworth, PL, Vassie, JM, Spencer, R, & Smith, DE. 1996. Precise datum control for pressure tide gauges. *Marine Geodesy*, **19**(1), 1–20.

Wöppelmann, G, & Marcos, M. 2016. Vertical land motion as a key to understanding sea level change and variability. *Reviews of Geophysics*, **54**(1), 64–92.

Yokoyama, Y, Esat, TM, Thompson, WG, Thomas, AL, Webster, JM, Miyairi, Y, Sawada, C, Aze, T, Matsuzaki, H, Okuno, J, *et al.* 2018. Rapid glaciation and a two-step sea level plunge into the Last Glacial Maximum. *Nature*, **559**(7715), 603–607.

Ringraziamenti

Un ringraziamento sentito al Professor Spada. Il percorso che ha portato a questo lavoro di tesi non è stato privo di ostacoli, ma è sempre stato una guida attenta e disponibile. Per gli stessi motivi, alla mia famiglia, è scontato ma senza il vostro sostegno non ce l'avrei fatta.

Grazie a Cece, Manu e Lele per i meme nei momenti più bui, e a Lele di nuovo per avermi imbruttito quando ne ho avuto bisogno. Al Bomps, per le infinite consulenze non retribuite, a Baffio, Purri, Giulia e Ross per esserci sempre stati. Non sarei la persona che sono senza di voi. A Celia, per essere un'amica migliore di quanto meriti. Ai Pippo Regaz, o come qualcuno li chiamerebbe, gli allegri compagni di merende, e a tutti i compagni di corso, di aule studio, di pause in questi anni. Siete troppi per citarvi tutti, ma sapete chi siete.

Una dedica ideale ad Alexandra Elbakyan, per essere un eroe contemporaneo, e una alla memoria di Richard Benson. Se un filosofo mi ha insegnato qualcosa, è stato lui.